

Ground-based validation of the Copernicus Sentinel-5p TROPOMI NO₂ measurements with the NDACC ZSL-DOAS, MAX-DOAS and Pandonia global networks

Tijl Verhoelst¹, Steven Compernolle¹, Gaia Pinardi¹, Jean-Christopher Lambert¹, Henk J. Eskes², Kai-Uwe Eichmann³, Ann Mari Fjæraa⁴, José Granville¹, Sander Niemeijer⁵, Alexander Cede^{6,7}, Martin Tiefengraber⁷, François Hendrick¹, Andrea Pazmiño⁸, Alkiviadis Bais⁹, Ariane Bazureau⁸, K. Folkert Boersma^{2,10}, Kristof Bognar¹¹, Angelika Dehn¹², Sebastian Donner¹³, Aleksandr Elokhov¹⁴, Manuel Gebetsberger⁷, Florence Goutail⁸, Michel Grutter de la Mora¹⁵, Aleksandr Gruzdev¹⁴, Myrto Gratsea¹⁶, Georg H. Hansen¹⁷, Hitoshi Irie¹⁸, Nis Jepsen¹⁹, Hugo Kanaya²⁰, Dimitris Karagkiozidis⁹, Rigel Kivi²¹, Karin Kreher²², Pieter Cornelius F. Levelt^{2,23}, Cheng Liu²⁴, Moritz Müller⁷, Monica Navarro Comas²⁵, Ankie J.M. Piters², Jean-Pierre Pommereau⁸, Thierry Portafaix²⁶, Cristina Prados-Roman²⁵, Olga Puentedura²⁵, Richard Querel²⁷, Julia Remmers¹³, Andreas Richter³, John Rimmer²⁸, Claudia Rivera Cárdenas¹⁵, Lidia Saavedra de Miguel¹², Valery P. Sinyakov²⁹, Wolfgang Stremme¹⁵, Kimberley Strong¹¹, Michel Van Roozendael¹, J. Pepijn Veefkind², Thomas Wagner¹¹, Folkard Wittrock³, Margarita Yela González²², and Claus Zehner¹⁰

¹Royal Belgian Institute for Space Aeronomy (BIRA-IASB), Ringlaan 3, 1180 Uccle, Belgium

²Royal Netherlands Meteorological Institute (KNMI), Utrechtseweg 297, 3730 AE De Bilt, The Netherlands

³Institute of Environmental Physics (IUP), University of Bremen, Otto-Hahn-Allee 1, D-28359 Bremen, Germany

⁴Norsk Institutt for Luftforskning (NILU), Instituttveien 18, 2007 Kjeller, Norway

⁵Science [&] Technology Corporation (S[&]T), Delft, The Netherlands

⁶Goddard Space Flight Center (NASA/GSFC), Greenbelt, MD, USA

⁷LuftBlick, Kreith, Austria & Institute of Meteorology and Geophysics, University of Innsbruck, Innsbruck, Austria

⁸Laboratoire Atmosphères, Milieux, Observations Spatiales (LATMOS), UVSQ Université Paris-Saclay/Sorbonne

Université/CNRS, Guyancourt, France

⁹Laboratory of Atmospheric Physics, Aristotle University of Thessaloniki (AUTH), Thessaloniki, Greece

¹⁰Meteorology and Air Quality group, Wageningen University, 6700 AA Wageningen, The Netherlands

¹¹Department of Physics, University of Toronto, 60 St. George Street, Toronto, Ontario, M5S 1A7, Canada

¹²European Space Agency/Centre for Earth Observation (ESA/ESRIN), Frascati, Italy

¹³Max-Planck-Institut für Chemie (MPI-C), Hahn-Meitner-Weg 1, 55128 Mainz, Germany

¹⁴A.M. Obukhov Institute of Atmospheric Physics (IAP), Russian Academy of Sciences, Moscow, Russian Federation

¹⁵Centro de Ciencias de la Atmósfera, Universidad Nacional Autónoma de México (UNAM), Mexico City, Mexico

¹⁶National Observatory of Athens, Lofos Nymphon - Thissio, PO Box 20048 - 11810, Athens, Greece

¹⁷Norsk Institutt for Luftforskning (NILU), P.O. Box 6606 Langnes, NO-9296 Tromsø, Norway

¹⁸Center for Environmental Remote Sensing, Chiba University (ChibaU), Chiba, Japan

¹⁹Danish Meteorological Institute (DMI), Lyngbyvej 100, 2100 Copenhagen, Denmark

²⁰Research Institute for Global Change (JAMSTEC), Yokohama, Japan

²¹Space and Earth Observation Centre, Finnish Meteorological Institute, Tähteläntie 62, FI-99600 Sodankylä, Finland

²²BK Scientific GmbH, Astheimerweg 42, 55130 Mainz, Germany

²³University of Technology Delft, Mekelweg 5, 2628 CD Delft, The Netherlands

²⁴Department of Precision Machinery and Precision Instrumentation, University of Science and Technology of China, Hefei, 230026, China

²⁵Atmospheric Research and Instrumentation, National Institute for Aerospace Technology (INTA), Madrid, 28850, Spain

²⁶Laboratoire de l'Atmosphère et des Cyclones (LACy), Université de La Réunion, Saint-Denis, France

²⁷National Institute of Water and Atmospheric Research (NIWA), Private Bag 50061, Omakau, Central Otago, New Zealand

²⁸University of Manchester, Oxford Rd, M13 9PL Manchester, United Kingdom

²⁹Kyrgyz National University of Jusup Balasagyn (KNU), 547 Frunze Str., Bishkek, Kyrgyz Republic

Correspondence: Tijl Verhoelst (tijl.verhoelst@aeronomie.be)

Abstract. This paper reports on consolidated ground-based validation results of the atmospheric NO₂ data produced operationally since April 2018 by the TROPOMI instrument on board of the ESA/EU Copernicus Sentinel-5 Precursor (S5p) satellite. Tropospheric, stratospheric, and total NO₂ column data from S5p are compared to correlative measurements collected from, respectively, 19 Multi-Axis DOAS (MAX-DOAS), 26 NDACC Zenith-Scattered-Light DOAS (ZSL-DOAS), and 25

5 PGN/Pandora instruments distributed globally. The validation methodology gives special care to minimizing mismatch errors due to imperfect spatio-temporal co-location of the satellite and correlative data, e.g., by using tailored observation operators to account for differences in smoothing and in sampling of atmospheric structures and variability, and photochemical modelling to reduce diurnal cycle effects. Compared to the ground-based measurements, S5p data show, on an average: (i) a negative bias for the tropospheric column data, of typically -23 to -37% in clean to slightly polluted conditions, but reaching values as high 10 as -51% over highly polluted areas; (ii) a slight negative bias for the stratospheric column data, of about -0.2 Pmolec/cm², i.e. approx. -2% in summer to -15% in winter; and (iii) a bias ranging from zero to -50% for the total column data, found to depend on the amplitude of the total NO₂ column, with small to slightly positive bias values for columns below 6 Pmolec/cm² and negative values above. The dispersion between S5p and correlative measurements contains mostly random components, 15 which remain within mission requirements for the stratospheric column data (0.5 Pmolec/cm²), but exceed those for the tropospheric column data (0.7 Pmolec/cm²). While a part of the biases and dispersion may be due to representativeness differences such as different area averaging and measurement times, it is known that errors in the S5p tropospheric columns exist due to shortcomings in the (horizontally coarse) a-priori profile representation in the TM5-MP chemistry transport model used in the S5p retrieval, and to a lesser extent, to the treatment of cloud effects and aerosols. Although considerable differences (up to 20 2 Pmolec/cm² and more) are observed at single ground-pixel level, the near-real-time (NRTI) and off-line (OFFL) versions of the S5p NO₂ operational data processor provide similar NO₂ column values and validation results when globally averaged, with the NRTI values being on average 0.79% larger than the OFFL values.

1 Introduction

Nitrogen oxides, and in particular the NOx (NO and NO₂), are important trace gases both in the troposphere and the stratosphere. In the troposphere they are produced mainly by the combustion of fossil and other organic fuels, and by the production 25 and use of nitrogen fertilizers for agriculture. They can also have a natural origin, e.g., lightning, biological processes in soils, and biomass burning. The NO/NO₂ ratio varies with solar illumination primarily, from 0.2-0.5 during the day down to zero at night. NOx are converted to nitric acid and nitrates, which are removed by dry deposition and rain, resulting in a tropospheric lifetime of a few hours to days. Tropospheric NOx are pollutants as well as proxies for other pollutants resulting from the

(high-temperature) combustion of organic fuels. They are precursors for tropospheric ozone and aerosols and contribute to acid rain and smog. Because of their adverse health effects, local to national regulations limiting boundary layer NO_x concentrations are now in place in a long list of countries across the world. In the stratosphere NO_x are formed by the photolysis of tropospheric nitrous oxide (N₂O) produced by biogenic and anthropogenic processes and going up through the troposphere and stratosphere. Stratospheric NO_x controls the abundance of ozone, as a catalyst in ozone destruction processes, but also by mitigating ozone losses caused by catalytic cycles involving anthropogenic halogens through the lock-up of these halogens in so-called long-lived reservoirs.

The global distribution, cycles and trends of atmospheric NO₂ have been measured from space by a large number of instruments on low-Earth orbit (LEO) satellites. Since the late 1970s, its stratospheric and sometimes mesospheric abundance has been measured by limb viewing and solar occultation instruments working in the UV-visible and infrared spectral ranges: SME, LIMS, SAGE(-II), HALOE, POAM-2/3... and, in the last decade, OSIRIS, GOMOS, MIPAS, SCIAMACHY, Scisat ACE, and SAGE-III. Follow-on missions combining limb and occultation measurements are in development, like ALTIUS planned for the coming years. Pioneered in 1995 with ERS-2 GOME (Burrows et al., 1999), which for the first time brought into space NO₂ column measurements by Differential Optical Absorption Spectroscopy (DOAS, Noxon et al. (1979); Platt and Perner (1983)), the global monitoring of tropospheric NO₂ has continued uninterruptedly with a suite of UV-visible DOAS instruments with improving sensitivity and horizontal resolution: Envisat SCIAMACHY (Bovensmann et al., 1999), EOS-Aura OMI (Levelt et al., 2018), and the series of MetOp-A/B/C GOME-2 (Valks et al., 2011; Liu et al., 2019b).

Owing to its cardinal role in air quality, tropospheric chemistry, stratospheric ozone, and as a precursor of essential climate variables (ECV), the monitoring of atmospheric NO₂ on a global scale has been given proper attention in the European Earth Observation programme Copernicus. The Copernicus Space Component (CSC) develops a constellation of atmospheric composition Sentinel satellites with complementary NO₂ measurement capabilities, consisting of Sentinel-4 geostationary missions (with hourly monitoring over Europe) and Sentinel-5 LEO missions (with daily monitoring globally) to be launched from 2023 onwards. A NO₂ measurement channel is also planned for the Copernicus Carbon Dioxide Monitoring mission CO2M for better attribution of the atmospheric emissions. First element in orbit of this LEO+GEO constellation, the TROPOspheric Monitoring Instrument (TROPOMI) was launched on board of ESA's Sentinel-5 Precursor (S5p) early-afternoon LEO satellite in October 2017. This hyperspectral imaging spectrometer measures the Earth radiance, at 0.2-0.4 nm resolution in the visible absorption band of NO₂, over ground pixels as small as $7.0 \times 3.5 \text{ km}^2$ or $5.5 \times 3.5 \text{ km}^2$ (before and after the switch to smaller pixel size on August 6, 2019, respectively) with an almost daily global coverage thanks to a swath width of 2600 km.

Pre-launch mission requirements for the Copernicus Sentinel NO₂ data are, for the tropospheric NO₂ column, a bias lower than 50% and an uncertainty lower than 0.7 Pmole/cm², and for the stratospheric NO₂ column, a bias lower than 10% and an uncertainty lower than 0.5 Pmole/cm² (ESA, 2017a, b). Since the beginning of its nominal operation in April 2018, in-flight compliance of S5p TROPOMI with these mission requirements has been monitored routinely by means of comparisons to ground-based reference measurements in the Validation Data Analysis Facility (VDAF) of the S5p Mission Performance Centre (MPC) and by confrontation with similar satellite data from OMI and GOME-2. The Copernicus S5p MPC routine operations validation service is complemented with ground-based validation studies carried out in the framework of ESA's

S5P Validation Team (S5PVT) through research projects funded nationally like NIDFORVAL (see details in the Acknowledgments section). Ground-based validation of satellite NO₂ data (e.g., Petritoli et al., 2003; Brinksma et al., 2008; Celarier et al., 2008; Ionov et al., 2008; Valks et al., 2011; Compernolle et al., 2020b; Pinardi et al., 2020) relies classically on three types of UV-visible DOAS instruments which, thanks to complementary measurement techniques, provide all together correlative observations sensitive to the three components of the S5p data product: Multi-Axis Differential Optical Absorption Spectroscopy (MAX-DOAS) measures the tropospheric column during the day, Zenith-Scattered-Light DOAS (ZSL-DOAS) the stratospheric column at dawn and dusk, and Pandora direct Sun instruments the total column during the day, respectively. Currently, those three types of instruments contribute to global monitoring networks. Fig. 1 shows the geographical distribution of instruments contributing data to the reported S5p validation study.

In this paper, we report on the consolidated results of the S5p NO₂ ground-based validation activities for the first two years of nominal operation. The TROPOMI tropospheric, stratospheric and total column data products under investigation are described in Sect. 2, with a brief assessment of the coherence between the data generated by the near-real-time (NRTI) and off-line (OFFL) channels of the operational processors. For clarity, we present in separate sections results for the stratospheric (Sect. 3), tropospheric (Sect. 4) and total (Sect. 5) NO₂ columns. These three sections include the description of the S5p data preparation, of the ground-based validation data, of the preparation of the filtered, co-located, and harmonized data pairs to be compared, and the comparison results. Robust, harmonised statistical estimators are derived from the comparisons consistently throughout the paper: the median difference as a proxy for the bias, and half of the 68% interpercentile (IP68/2) as a measure of the comparison spread (equivalent to a standard deviation for a Normal distribution, but much less sensitive to unavoidable outliers). Thereafter, in Sect. 6, these individual results are assembled and discussed all together, to derive conclusions on their mutual coherence, on the fitness-for-purpose of the S5p data, and on remaining challenges for the accurate validation of NO₂ observations from space.

85 2 S5p TROPOMI data

2.1 Data description and filtering

The retrieval of NO₂ (sub)columns from TROPOMI Earth nadir radiance and solar irradiance spectra is a 3-step process relying on DOAS and on a Chemical Transport Model (CTM) based stratosphere-troposphere separation. The TROPOMI NO₂ algorithm is an adaptation of the QA4ECV community retrieval approach (Boersma et al. (2018)) and of the DOMINO/TEMIS algorithm (Boersma et al., 2007, 2011), already applied successfully to heritage and current satellite data records (GOME, SCIAMACHY, OMI, GOME-2). In the first step, the integrated amount of NO₂ along the optical path, or slant column density (SCD), is derived using the classical DOAS approach (Platt and Perner, 1983). In the second step, the retrieved SCD is assimilated by the TM5-MP CTM to allocate a vertical profile of the NO₂ concentration, needed for the separation between stratospheric and tropospheric SCDs. This assimilation procedure favours observations over pristine, remote areas where the entire NO₂ SCD can be attributed to the stratospheric component. Assuming relatively slow changes in the stratospheric NO_x field, the model transports information to areas with a more significant tropospheric component. In the third step, the three

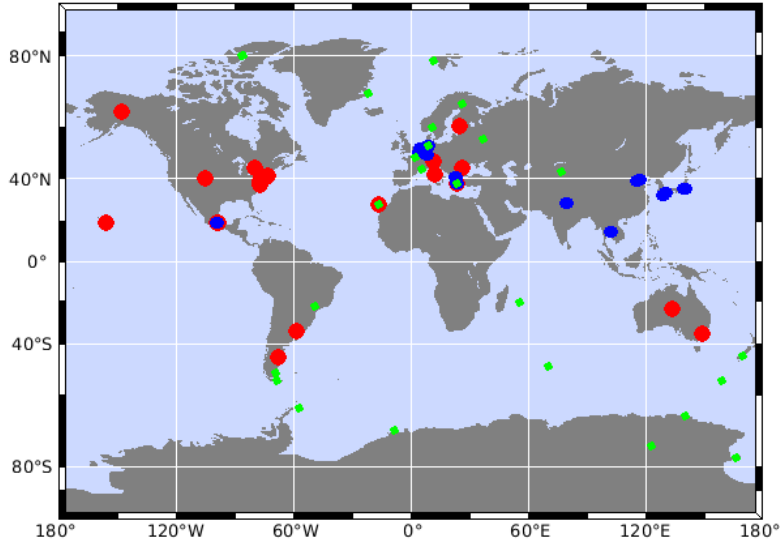


Figure 1. Geographical distribution of the UV-visible DOAS spectrometers contributing the ground-based correlative measurements: 26 NDACC ZSL-DOAS instruments in green, 19 MAX-DOAS instruments in blue, and 25 PGN instruments in red.

slant (sub)column densities are converted into vertical (sub)column densities using appropriate Air Mass Factors (AMFs). The CTM can be run either in forecast mode, using 1-day forecast meteorological data from the European Centre for Medium-range Weather Forecasts (ECMWF), or in a more delayed processing mode, using 0-12hour forecast meteorological data. The former 100 is used for near-real-time (NRTI) processing of the TROPOMI measurements, the latter for the offline (OFFL) production. For full technical details, the reader is referred to the Product Readme File (PRF), Product User Manual (PUM) and Algorithm Theoretical Basis Document (ATBD), all available at <http://www.tropomi.eu/data-products/nitrogen-dioxide>. A detailed description and quality assessment of the derived slant column data is already published by van Geffen et al. (2020), and a publication on satellite inter-comparison of vertical column data is under preparation (Eskes et al., 2020). The current paper 105 addresses the independent ground-based validation of vertical sub-column densities in the troposphere and stratosphere and of the vertical total column. The S5p data set validated here covers the nominal operational phase (Phase E2) of the S5p mission, starting in April 2018 and up to February 2020. No data obtained during the commissioning phase of the satellite have been used. Table 1 provides an overview of the processor versions to which this corresponds. They constitute as continuous a data set as possible from May (NRTI) or October (OFFL) 2018 onward. Combining RPRO (May-October 2018) with OFFL, a 110 coherent dataset with version OFFL processor v01.02.02 or higher can be obtained.

Table 1. Identification of the S5p NO₂ data versions validated here: near-real-time channel (NRTI), off-line channel (OFFL) and interim reprocessing (RPRO). Major updates were those leading to v01.02.00 and to v01.03.00.

Processor version	start orbit	start date	end orbit	end date
NRTI				
01.00.01	2955	2018-05-09	3364	2018-06-07
01.00.02	3745	2018-07-04	3946	2018-07-18
01.01.00	3947	2018-07-18	5333	2018-07-24
01.02.00	5336	2018-10-24	5929	2018-12-05
01.02.02	5931	2018-12-05	7517	2019-03-27
01.03.00	7519	2019-03-27	7999	2019-03-30
01.03.01	7999	2019-03-30	9158	2019-07-20
01.03.02	9159	2019-07-20	current version	
OFFL				
01.02.00	5236	2018-10-17	5832	2018-11-28
01.02.02	5840	2018-11-29	7424	2019-03-20
01.03.00	7425	2019-03-20	7906	2019-04-23
01.03.01	7907	2019-04-23	8814	2019-06-26
01.03.02	8815	2019-06-26	current version	
RPRO				
01.02.02	2836	2018-05-01	5235	2018-10-17

Besides very detailed quality flags, the S5p NO₂ data product includes a combined quality assurance value (qa_value) enabling end users to easily filter data for their own purpose. For tropospheric applications (when not using the averaging kernels), the guideline is to use only NO₂ data with a qa_value > 0.75. This removes very cloudy scenes (cloud radiance fraction > 0.5), snow- or ice-covered scenes, and problematic retrievals. For stratospheric applications, where clouds are less of an issue, a more relaxed threshold of qa_value > 0.5 is recommended. These data filtering recommendations have been applied here, where the stricter requirement of qa_value > 0.75 has been used for the total column validation as well. Again, further details on this can be found in the PRF, PUM, and ATBD.

2.2 Mutual coherence between NRTI and OFFL

As described in Sect. 2.1, the main difference between the NRTI and OFFL data processors lies in the use of either forecast or analysis ECMWF meteorological data as input, and consequently the use of either forecast or analysis TM5-MP vertical NO₂ profiles. The mutual consistency between the NRTI and OFFL data products is monitored routinely using data and tools provided by the S5p MPC Level-2 Quality Control Portal (<https://mpc-l2.tropomi.eu>). Fig. 2 shows that, looking at global means of the NO₂ total column, the NRTI and OFFL data look very much alike, with NRTI column values on an average

0.79% larger than those obtained in OFFL. Eight NRTI and six OFFL processor versions are used in this comparison (as identified in Table 1). The activation of the successive processor versions and the switch to the smaller ground pixel size (on August 6, 2019) are marked by the yellow vertical lines. As expected both NRTI and OFFL channels show NO₂ maxima in the winter/summer seasons (December, June) and minima near the equinoxes. The scatter also exhibits a seasonal cycle, with largest values observed in the Northern Hemisphere winter season.

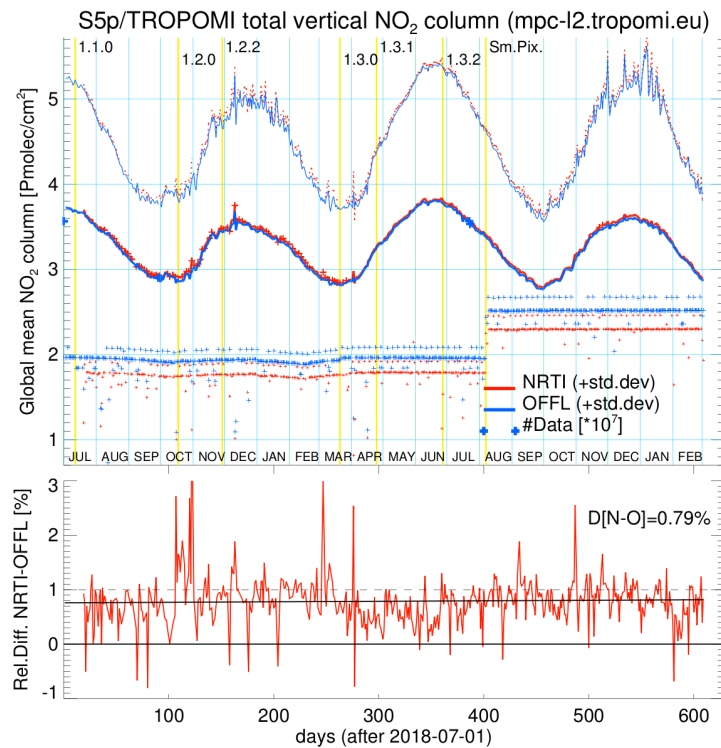


Figure 2. *Upper panel:* Time series of the global means of NO₂ total column data retrieved with the NRTI (red line) and OFFL (blue line) processors, and their standard deviation, in Pmolec/cm², from July 2018 till February 2020. Crosses depict the number of measurements divided by 10⁷, with the same colour code: red for NRTI, blue for OFFL. Yellow vertical lines indicate the transition dates for processor upgrades and the switch to the smaller ground pixel size. *Lower panel:* Percent relative difference between NRTI and OFFL global means of total NO₂ values. The Theil-Sen linear regression line (black) is superimposed.

To further assess similarities and differences between the NRTI and OFFL processing channels, NO₂ values along individual 130 orbits are also compared directly. An illustration is given in Figure 3 for S5p orbit #07407, a randomly selected orbit crossing Western Europe on a relatively cloud-free day (March 19, 2019).

The three maps of Figure 3 show the difference between NRTI and OFFL values for the total, stratospheric and tropospheric NO₂ column, respectively, together with the corresponding Pearson correlation coefficient and root-mean-square deviation (RMSD). While the correlation coefficient is high (typically around 0.97), the maps do reveal regions where significant de-

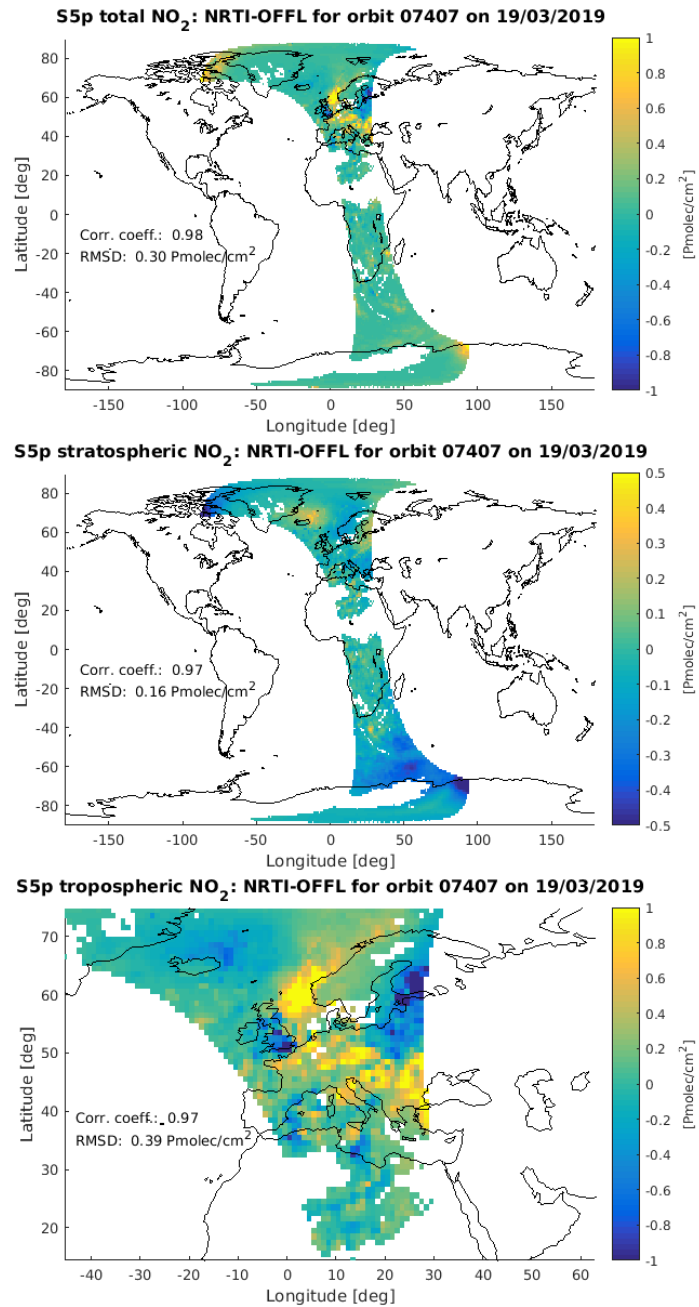


Figure 3. Maps of the difference between the NRTI and OFFL NO₂ data values for S5p orbit #07407 on March 19, 2019. *Upper panel:* difference between total column values; *Middle panel:* stratospheric columns; *Lower panel:* zoom on the difference in tropospheric column values over Western Europe.

135 viations occur, up to ± 0.5 Pmolec/cm 2 between the NRTI and OFFL stratospheric columns, and up to ± 2 Pmolec/cm 2 for both the tropospheric columns and the total columns. Significant differences over South-East England (London) and in the Manchester-Liverpool area are particularly striking. North-East of Iceland, NRTI-OFFL differences in stratospheric and in tropospheric columns are of opposite sign, indicating a different stratosphere/troposphere separation after the slant column retrieval leading to little difference in the total columns. A more detailed investigation targeted solely at regions and times of
140 significant deviations between NRTI and OFFL would be needed to better reveal the full benefit of the OFFL analysis, but that is beyond the scope of the current paper. What needs to be underlined is that the ground-based validation studies on which the present consolidated results are based upon, do not yield significantly different conclusions for the two processing modes. Therefore, all results reported in this paper may be considered as applicable to the two processing channels.

3 Stratospheric column validation

145 3.1 NDACC Zenith-sky DOAS data

Since the pioneering ages of NO₂ column measurements from space with ERS-2 GOME in the mid-1990s, ground-based UV-visible DOAS measurements at twilight have served as a reference for the validation of NO₂ total column data over unpolluted stations and of NO₂ stratospheric column data from all nadir UV-visible satellites to date (e.g., Lambert et al., 1997a, b; Petritoli et al., 2003; Celarier et al., 2008; Ionov et al., 2008; Gruzdev and Elokhov, 2010; Dirksen et al., 2011; Hendrick et al., 2011; Robles-Gonzalez et al., 2016). Here as well, S5p TROPOMI stratospheric NO₂ column data are compared to the correlative measurements acquired by ZSL-DOAS (Zenith-Scattered Light Differential Optical Absorption Spectroscopy) UV-Visible spectrometers (e.g. Solomon et al., 1987; Hendrick et al., 2011, and references therein). A key property of zenith-sky measurements at twilight is the geometrical enhancement of the optical path in the stratosphere (Solomon et al., 1987), which offers high sensitivity to stratospheric absorbers of visible radiation and lower sensitivity to clouds and tropospheric species (except in the case of strong pollution events during thunderstorms or thick haze, see e.g. Pfeilsticker et al. (1999)). However, the geometrical enhancement also implies horizontal smoothing of the measured information over hundreds of kilometres, which requires appropriate co-location methods to avoid large discrepancies with the higher-resolution measurements of TROPOMI, as discussed in Sect. 3.2. Various ZSL-DOAS UV-visible instruments with standard operating procedures and harmonized retrieval methods perform network operation in the framework of the Network for the Detection of Atmospheric
150 Composition Change (NDACC, De Mazière et al. (2018)). Part of this, over 15 instruments of the SAOZ design (Système d'Analyse par Observation Zénitale) are distributed worldwide and provide data in near-real-time through the CNRS LATMOS_RT Facility (Pommereau and Goutail, 1988). For the current work, ZSL-DOAS validation data have been obtained: (1) through the LATMOS_RT Facility (in nearl-real-time processing mode), (2) from the NDACC Data Host Facility (DHF), and (3) via private communication with the instrument operator. The geographical distribution of these instruments is shown in
155 Fig. 1 and further details are provided in A1 in the supplement. Measurements are made during twilight, at sunrise and sunset, but only sunset measurements are used here for signal-to-noise reasons (larger NO₂ column) and as these happen closer in time to the early-afternoon overpass of S5p. NDACC intercomparison campaigns (Roscoe et al., 1999; Vandaele et al., 2005) con-

clude to an uncertainty of about 4-7% on the slant column density. After conversion of the slant column into a vertical column using a zenith-sky AMF, and for the latest version of the data processing, the uncertainty on the vertical column is estimated 170 to be the order of 10-14% (Yela et al., 2017; Bognar et al., 2019). A limiting factor comes from the temperature dependence of the NO₂ absorption cross-sections used in the DOAS retrieval of the slant column density. Most of the NDACC instruments use cross-sections at a single temperature (220 K), which introduces a seasonal error of up to a few percent at middle and high latitudes.

3.2 Co-location and harmonization

175 To account for effects of the photochemical diurnal cycle of stratospheric NO₂, the ZSL-DOAS measurements at sunset are adjusted to the early-afternoon S5p overpass time using a model-based correction factor. The latter is calculated with the PSCBOX 1D stacked-box photochemical model (Errera and Fonteyn, 2001; Hendrick et al., 2004) initiated by daily fields from the SLIMCAT chemistry-transport model (CTM). The amplitude of the adjustment factor is sensitive to the effective SZA assigned to the ZSL-DOAS measurements. It is assumed here to be 89.5° or, during polar day and close to polar night, 180 the largest or smallest SZA reached, respectively. The uncertainty related to this adjustment is estimated to be of the order of 10%, the main source of uncertainty probably being the effective SZA to assign to the full twilight measurement period. To reduce mismatch errors due to the significant difference in horizontal sensitivity between S5p and ZSL-DOAS measurements, individual TROPOMI NO₂ stratospheric column data (in ground pixels at high horizontal sampling) are averaged over the much larger footprint of the air mass to which the ground-based zenith-sky measurement is sensitive, see Lambert et al. 185 (1997b, ISBN 978-1-4614-3908-0, © Springer New York, 2012); Verhoelst et al. (2015) and Compernolle et al. (2020b) for details. The length of this footprint is of the order of 300-600 km in the direction of the sun, and the width is typically of the order of 50-100 km at mid latitudes, depending on the duration of sunrise and sunset. Note that, as the TROPOMI stratospheric column is a TM5 output, its true resolution is actually much lower than the pixel size.

3.3 Comparison results

190 Fig. 4 illustrates the comparison between TROPOMI and ground-based ZSL-DOAS SAOZ NO₂ data at the NDACC station at Observatoire de Haute Provence (O.H.P.) in Southern France. The time series reveal a small negative median difference for TROPOMI, which is found to be a common feature across the network, but little seasonal structure. The correlation coefficient is excellent and the histogram of the differences has an almost Gaussian shape.

195 Comparison results for the entire ZSL-DOAS network are presented in Fig. 5. This figure reveals occasionally larger differences in more difficult co-location conditions (e.g. enhanced variability at the border of the polar vortex) but no impact of the TROPOMI pixel size change on August 6th, 2019. The latter result must be interpreted with care as, for these comparisons, multiple TROPOMI pixels are averaged over the ZSL-DOAS observation operator before comparison (see Sect. 3.2), and as such any change in the noise statistics of individual pixels will be hidden.

200 Statistical estimators of the bias (median difference) and scatter per station are presented in box-whisker plots in Fig. 6, and in tabular form in A1. Across the network, S5p NRTI and OFFL stratospheric NO₂ column data are generally lower than the

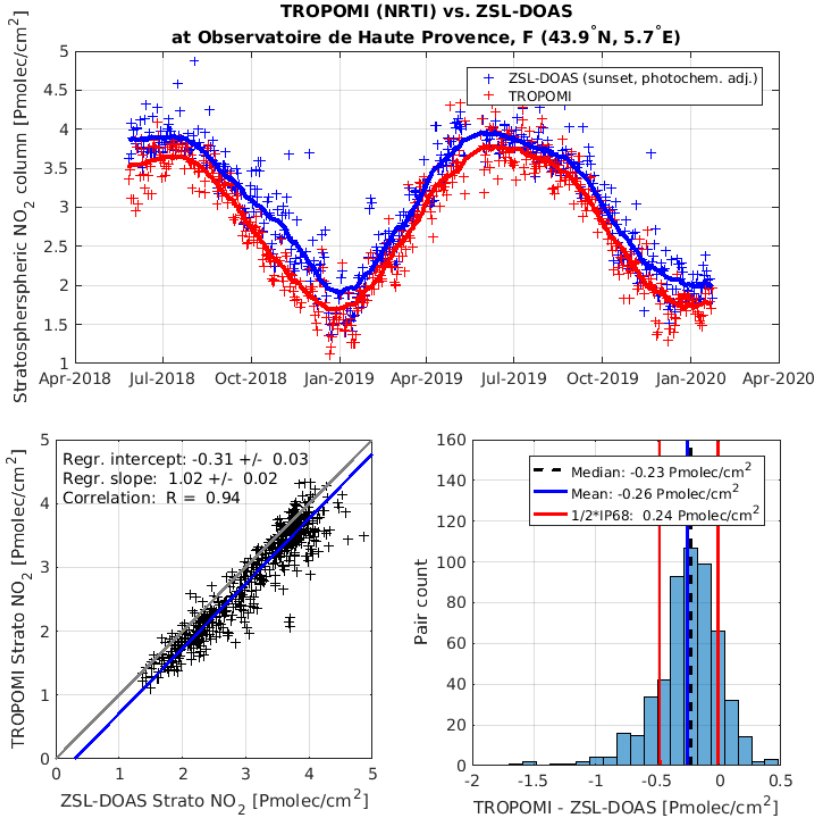


Figure 4. *Upper panel:* Time series of S5p NRTI stratospheric NO_2 column data co-located with ground-based SAOZ sunset measurements performed by CNRS/LATMOS at the NDACC mid-latitude station of Observatoire de Haute-Provence (France). The latter were adjusted for the photochemical difference between the S5p and twilight solar local times, while S5p data were averaged over the ground-based twilight air mass. Solid lines represent 2-month running medians. *Lower panels:* Scatter plot (left-hand side) and histogram of the difference (right-hand side) with several statistical measures of the agreement between data.

ground-based values by approximately 0.2 Pmole/cm², with a station-to-station scatter of this median difference of similar magnitude (0.3 Pmole/cm²). These numbers are within the mission requirement of a maximum bias of 10% (equivalent to 0.2-0.4 Pmole/cm², depending on latitude and season), and within the combined systemic uncertainty of the reference data and their model-based photochemical adjustment. The IP68/2 dispersion of the difference between TROPOMI stratospheric 205 column and correlative data around their median value rarely exceeds 0.3 Pmole/cm² at sites without tropospheric pollution. When combining random errors in the satellite and reference measurements with irreducible co-location mismatch effects, it can be concluded that the random uncertainty on the S5p stratospheric column measurements falls within mission requirements of max. 0.5 Pmole/cm² uncertainty.

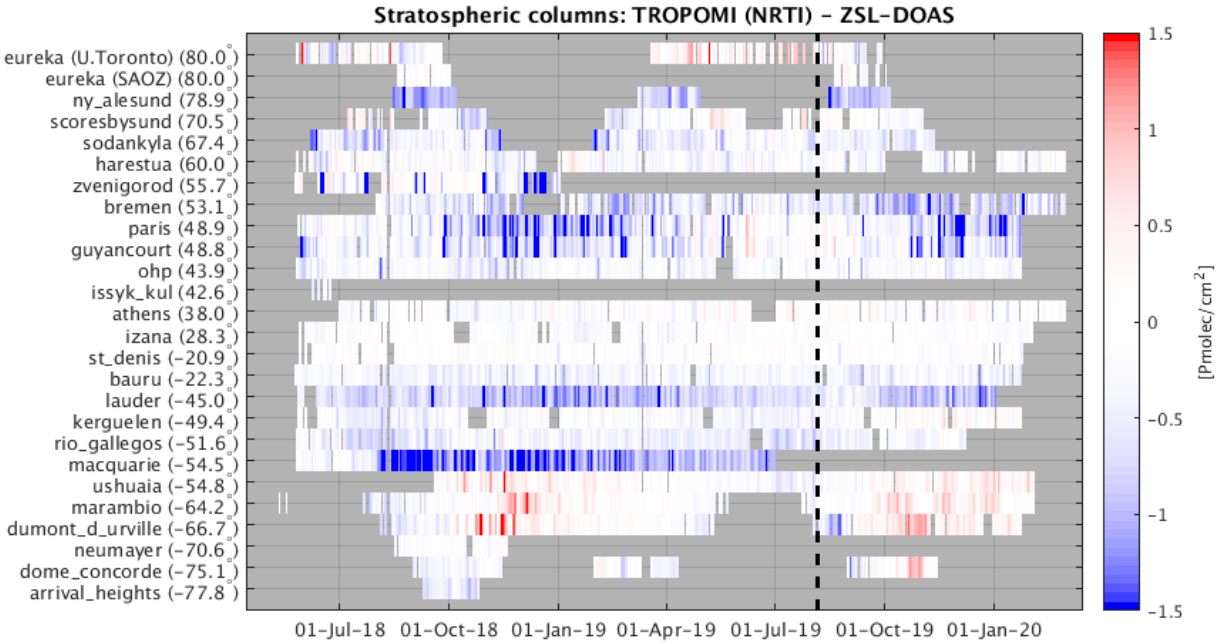


Figure 5. Difference between the S5p TROPOMI and NDACC ZSL-DOAS NO₂ stratospheric column data as a function of time, after photo-chemical adjustment of the ZSL-DOAS sunset data to the S5p SZA. Stations are ordered by increasing latitude (South at the bottom). The dashed vertical line on August 6, 2019, represents the reduction in S5p ground pixel size from $7.0 \times 3.5 \text{ km}^2$ to $5.5 \times 3.5 \text{ km}^2$.

The potential dependence of the TROPOMI stratospheric column bias and uncertainty on several influence quantities has
 210 been evaluated. Fig. 7 shows results for the solar zenith angle (SZA), the fractional cloud cover (CF), and the surface albedo of the TROPOMI measurement. This evaluation does not reveal any variation of the bias much larger than 0.4 Pmolec/cm² over the range of those influence quantities.

3.4 PGN measurements at high-altitude stations

Three of the PGN direct-sun instruments (see Sect. 5) are located near the summit of a volcanic peak: Altzomoni (3985m
 215 a.m.s.l) in the State of Mexico, Izaña (2360m a.m.s.l.) on Mount Teide on the island of Tenerife, and Mauna Loa (4169m a.m.s.l.) on the island of Hawaii. At these high-altitude sites the total column measured by the ground-based direct-sun instrument misses most of the tropospheric (potentially polluted) part and as such becomes representative of the TROPOMI stratospheric column. These sites have therefore been added to Fig. 6, illustrating that these comparisons based on direct-sun data yield similar conclusions as those based on zenith-sky data, that is, a minor negative median difference of the order of
 220 -0.2 Pmolec/cm². It must be noted that the PGN data are processed using cross sections at a single temperature, representative

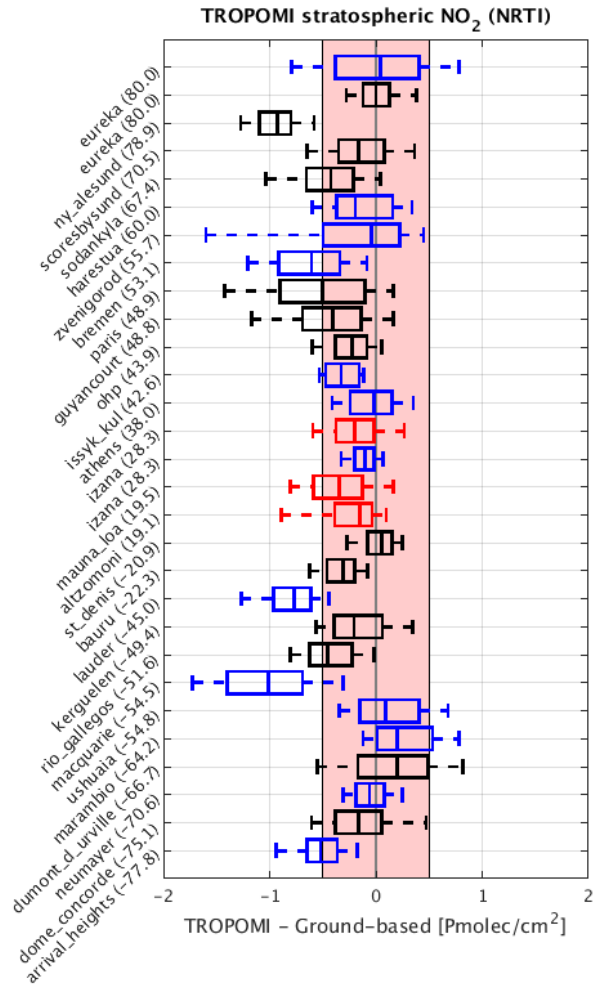


Figure 6. Box-and-whisker plots summarizing from pole to pole the bias and spread of the difference between S5p TROPOMI NRTI and NDACC ZSL-DOAS NO₂ stratospheric columns (SAOZ data in black, other ZSL-DOAS in blue, and PGN in red). The median difference is represented by a vertical solid line inside the box, which marks the 25 and 75% quantiles. The whiskers cover the 9-91% range of the differences. The shaded area represents the mission requirement of 0.5 Pmole/cm² for the uncertainty. Values between brackets in the labels denote the latitude of the station.

for the troposphere (254 K). This leads to columns which are about 10% larger than if they had been processed with cross sections for 220 K. Future processing of the PGN data will address this, and it is expected that this will mostly remove the apparent negative bias for TROPOMI (but lead to a slight inconsistency with the ZSL-DOAS results).

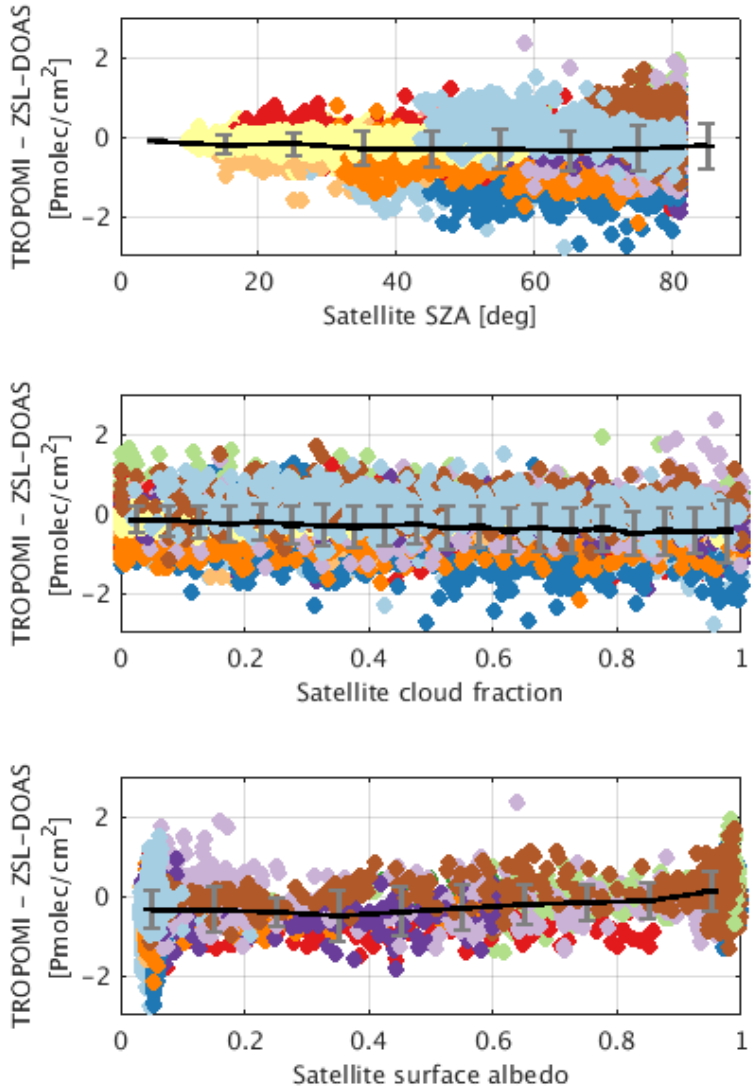


Figure 7. Dependence of the difference between TROPOMI NRTI and ground-based ZSL-DOAS stratospheric NO₂ column data on the satellite solar zenith angle (SZA), satellite cloud fraction, and satellite surface albedo, including a median and IP68/2 spread per bin (bin widths of 10 degrees in SZA, 0.05 in CF, and 0.1 in surface albedo). Different colours represent different stations, to illustrate the (modest) impact of station-to-station network in-homogeneity on these analyses.

4 Tropospheric column validation

225 4.1 MAX-DOAS data

Satellite tropospheric NO₂ column data are compared clasically to correlative measurements acquired by MultiAxis-Differential Optical Absorption Spectroscopy (MAX-DOAS) instruments (Hönninger and Platt, 2002; Honninger et al., 2004;

Sinreich et al., 2005). MAX-DOAS instruments measure from sunrise to sunset the UV-visible radiance scattered in several directions and elevation angles, from which the tropospheric VCD and/or the lowest part of the tropospheric NO₂ profile (usually up to 3km altitude, and up to 10km at best) can be retrieved through different techniques (see e.g. Clémer et al., 2010; Hendrick et al., 2014; Friedrich et al., 2019; Bösch et al., 2018; Irie et al., 2008, 2011; Vlemmix et al., 2010; Wagner et al., 2011; Beirle et al., 2019), with between 1 and 3 degrees of freedom. Their horizontal spatial representativeness varies with the aerosol load and the spectral region of the retrieval, from a few km to tens of km (Irie et al., 2011; Wagner et al., 2011; Wang et al., 2014). Published total uncertainty estimates on the NO₂ tropospheric VCD are of the order of 7-17% in polluted conditions, including both random (around 3 to 10% depending on the instrument) and systematic (11 to 14%) contributions (Irie et al., 2011; Wagner et al., 2011; Hendrick et al., 2014; Kanaya et al., 2014). These ranges are more or less confirmed by the uncertainties reported in the data files, as visualized in Fig. A1 in the supplement. Nevertheless, differences in the reported uncertainties and in the actual measurement of the same scene between individual instruments are sometimes larger and the main potential sources of these inhomogeneities are summarized below:

– Different uncertainty reporting strategy: the reported systematic uncertainty may include only that from the NO₂ cross sections (approx. 3%; UNAM, BIRA-IASB, MPIC, AUTH, IUPB) or it may include also a contribution from the VCD retrieval step (up to 14% in JAMSTEC data and 20% in KNMI data) and the aerosol retrieval (Chiba-U Irie et al., 2011).

– Different SCD retrieval: Recommended common DOAS settings are used by all groups in the present study, and when doing so, instrument intercomparison campaigns like CINDI-1 and -2 (Roscoe et al., 2010; Kreher et al., 2020) revealed relative biases between 3 and 10% in DSCD.

– Different methods to retrieve VCD from DSCD (see also Table A2): Using either (1) vertical profile inversion using optimal estimation (BIRA-IASB, UNAM), (2) profile inversion using (an optimal estimation of) parameterized profile shapes (JAMSTEC and Chiba-U), (3) direct retrieval via the calculation of a tropospheric AMF (QA4ECV datasets), or (4) direct retrieval using a geometrical approximation, can lead to systematic differences in the 5-15% range (Vlemmix et al., 2015; Frieß et al., 2019).

Consequently, expert judgment on the total uncertainty at the network level yields a conservative estimate of 30% uncertainty in polluted conditions. Ongoing efforts to harmonise MAX-DOAS tropospheric NO₂ data processing, e.g. as part of the ESA FRM4DOAS project, should help minimizing such network inhomogeneities in the near future.

MAX-DOAS data have been used extensively for tropospheric NO₂ satellite validation, for instance for Aura OMI and MetOp GOME-2 (e.g. by Celarier et al., 2008; Irie et al., 2012; Lin et al., 2014; Kanaya et al., 2014; Wang et al., 2017; Drosoglou et al., 2018; Liu et al., 2019a; Compernolle et al., 2020b; Pinardi et al., 2020), as well as for the evaluation of modelling results (Vlemmix et al., 2015; Blechschmidt et al., 2020).

Data are collected either through ESA's Atmospheric Validation Data Centre (EVDC, <https://evdc.esa.int/>) or by direct delivery from the instrument Principal Investigators (e.g. within the S5PVT NIDFORVAL AO project). Currently, 19 MAX-DOAS stations have contributed correlative data in the TROPOMI measurement period from April 2018 to February 2020. Detailed

information about the stations and instruments is provided in A2. A few contributing sites measure in several geometries (e.g., Xianghe measure in both MAX-DOAS and direct sun mode, Bremen and Athens both report MAX-DOAS and zenith-sky measurements) or have multiple instruments (e.g., Cabauw and UNAM stations host both MAX-DOAS and Pandora instruments). This allows detailed (sub)column consistency-checks and in-depth analysis of the site peculiarities, out of the scope of 265 the present overview paper.

4.2 Co-location and harmonization

TROPOMI data is filtered following the $qa_value > 0.75$ rule as recommended in the associated PRF (see Sect. 2). Then for each day, the pixel over the site is selected. MAX-DOAS data series are temporally interpolated at the TROPOMI overpass time (only if data within ± 1 h exist) and daily comparisons are performed. This short temporal window avoids the need for a 270 photochemical cycle adjustment. Details on the comparison approach are described in Pinardi et al. (2020) for the validation of OMI and GOME-2 NO₂ column data and in Compernolle et al. (2020b) for the validation of the OMI QA4ECV NO₂ Climate Data Record.

4.3 Comparison results

An illustration of the daily comparisons between TROPOMI and ground-based MAX-DOAS measurements between May 275 2018 and end of January 2020, is presented in Fig. 8 for the Uccle station (Brussels, B, with moderate pollution levels). The two datasets have a correlation coefficient of 0.75 and a regression slope and intercept of 0.47 and 1.0 Pmolec/cm² respectively. The (median and mean) difference of about -2.3 to -3.1 Pmolec/cm² corresponds to a median relative difference of about -30%.

Results for the entire MAX-DOAS network are presented in Fig. 9. This figure reveals mostly (but not only) negative differences with a fairly significant variability but no clear seasonal features. No impact of the TROPOMI ground pixel size change 280 on August 6, 2019, is observed.

Box-whisker plots for the whole network are shown in Fig. 10, with corresponding numeric values listed in A2. Based on measurements from these 19 MAX-DOAS stations, three different regimes can be identified:

(i) Small tropospheric NO₂ column values (median values below 2 Pmolec/cm²), e.g. at the Fukue and Phimai stations, lead to small differences. Typically, these stations show a small median biase (<0.5 Pmolec/cm²), but these can still correspond to 285 up to a -27% relative bias. The dispersion (IP68/2) of the difference is smaller than 1 Pmolec/cm².

(ii) More polluted sites (median tropospheric columns from 3 to 14 Pmolec/cm²) experience a clear negative bias. The median difference ranges between -1 and -5 Pmolec/cm², i.e. between -15% (Chiba) and -56% (Pantnagar). This underestimation is similar to the one identified in the validation of Aura OMI and MetOp GOME-2 tropospheric NO₂ data by Compernolle et al. (2020b) and Pinardi et al. (2020). The dispersion (IP68/2) of the difference ranges from ~2 to ~6 Pmolec/cm², roughly 290 increasing with increasing tropospheric NO₂ median VCD.

(iii) Extremely polluted sites report larger differences. This is the case e.g. at the Mexican UNAM sites (UNAM and Vallejo in/close to Mexico city, and Cuautitlan in a more remote part of the state of Mexico), with median tropospheric columns larger

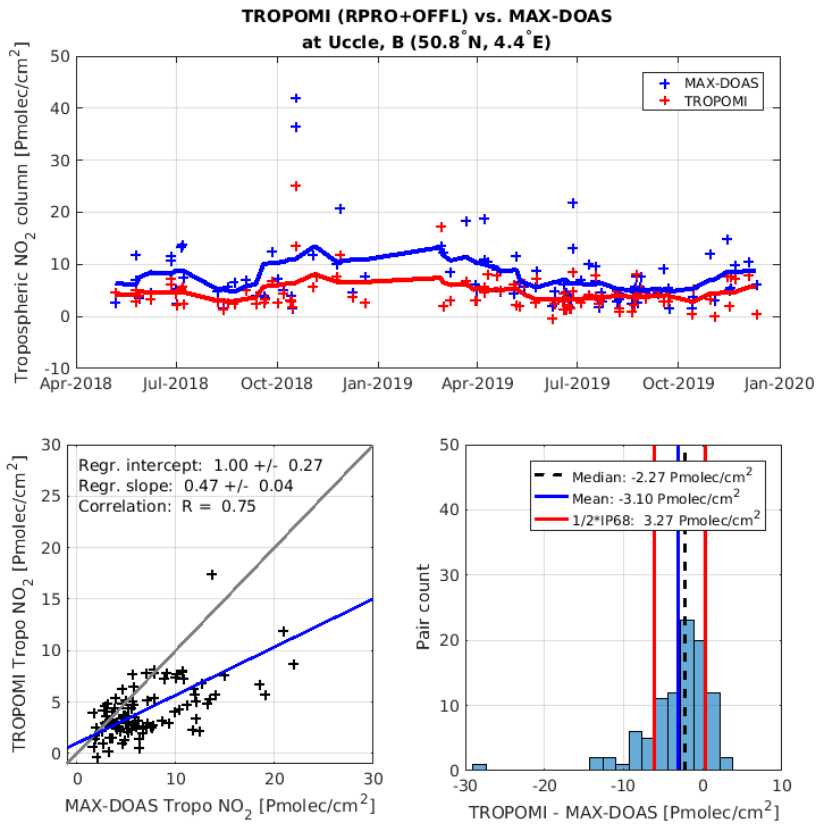


Figure 8. Same as Fig. 4, but now for the S5p OFFL tropospheric NO₂ column data co-located with ground-based MAX-DOAS measurements performed by BIRA-IASB at the NDACC mid-latitude station of Uccle in Brussels (Belgium).

than 15 Pmole/cm². These stations experience larger differences (>10 Pmole/cm², i.e., from -37 to -74%). The dispersion (IP68/2) of the difference is also quite large, between 4 and ~12 Pmole/cm². Results at these sites need deeper analysis.

295 The overall bias (median of all station median differences) is -2.4 Pmole/cm², i.e. -37%. The median dispersion is 3.5 Pmole/cm² while the site-to-site dispersion (IP68/2 over all site medians) is 2.8 Pmole/cm². Note that these network-averaged numbers are close to the numbers found for the polluted (Athens to Gucheng) sites. These results are within the mission requirement of a maximum bias of 50%, but they exceed the uncertainty requirement of at most 0.7 Pmole/cm² which is only satisfied for the clean-sites ensemble. A discussion on the causes of these biases and sometimes large comparisons spread is provided in Sect. 6.

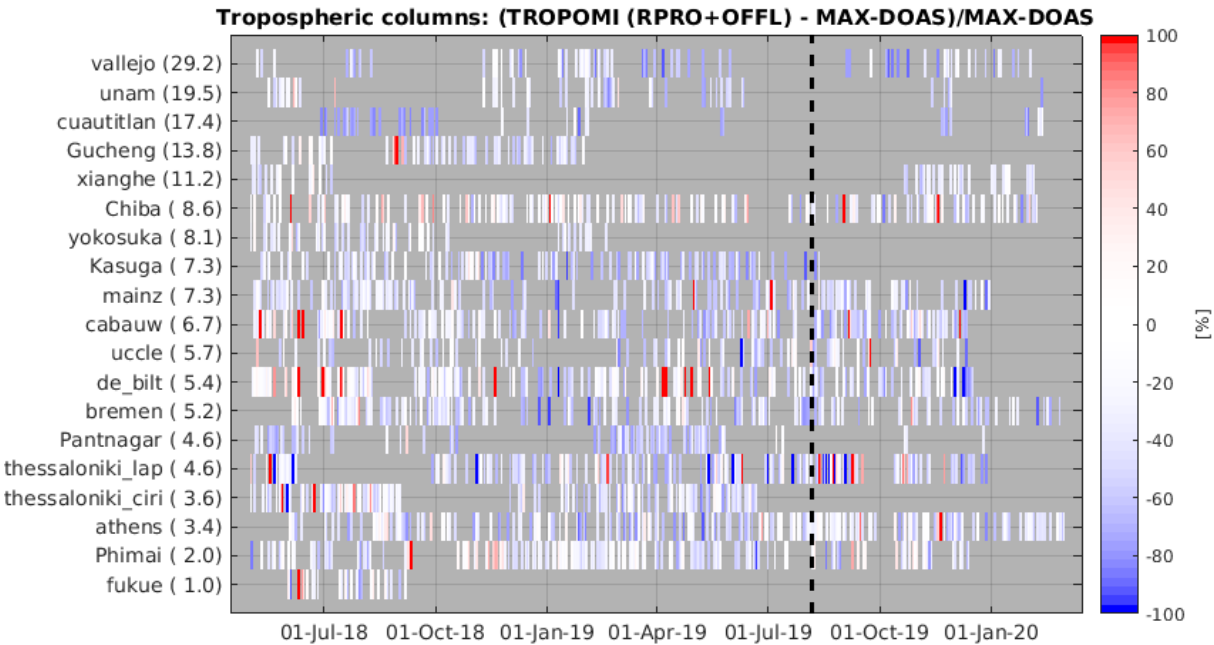


Figure 9. Percent relative difference between the S5p TROPOMI and MAX-DOAS NO₂ tropospheric column data as a function of time. Stations are ordered by median NO₂ tropospheric column (lowest median value at the bottom). The dashed vertical line on August 6, 2019, represents the reduction in S5p ground pixel size from $7.0 \times 3.5 \text{ km}^2$ to $5.5 \times 3.5 \text{ km}^2$.

5 Total column validation

5.1 PGN/Pandora data

The Pandoria Global Network (PGN) delivers direct-sun total column and multi-axis tropospheric column observations of several trace gases including NO₂ from a network of ground-based standardized Pandora sunphotometers in an automated 305 way. In this work, only direct-sun observations are used. These have a random error uncertainty of about 0.27 Pmolec/cm² and a systematic error uncertainty of 2.7 Pmolec/cm² (Herman et al., 2009). Studies at US and Korean sites during DISCOVER-AQ campaign found a good agreement of Pandora instruments with aircraft in-situ measurements (within 20 percent on average Choi et al., 2019), although larger differences are observed for individual sites (Nowlan et al., 2018).

Pandora data have been used before to validate satellite NO₂ measurements from Aura OMI (Herman et al., 2009; Tzortziou 310 et al., 2014; Kollonige et al., 2018; Choi et al., 2019; Judd et al., 2019; Griffin et al., 2019; Herman et al., 2019; Pinardi et al., 2020) and TROPOMI (Griffin et al., 2019; Ialongo et al., 2020; Zhao et al., 2019).

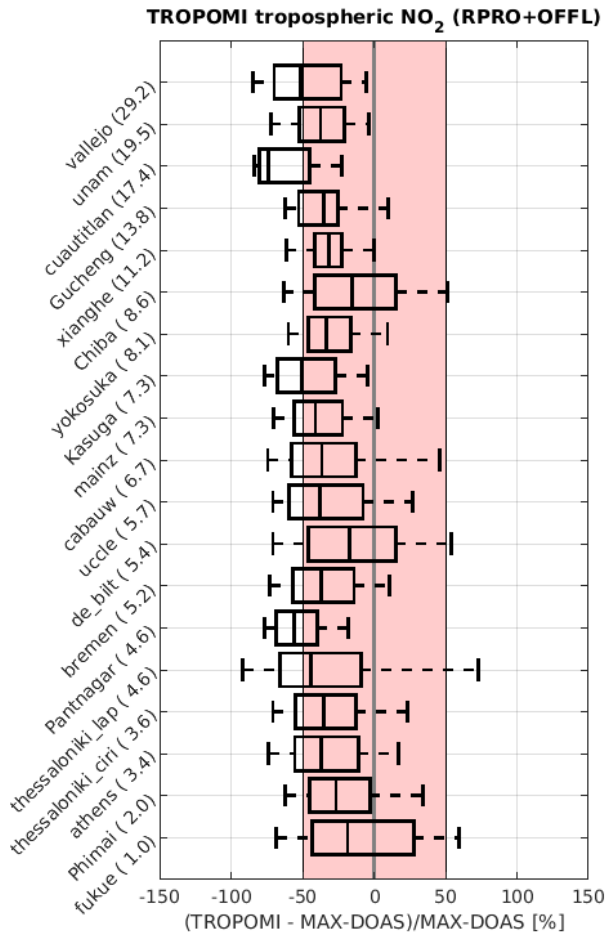


Figure 10. Same as Fig. 6, but now for the difference between S5p TROPOMI OFFL and MAX-DOAS NO₂ tropospheric columns, and with ordered as a function of the median ground-based tropospheric column (largest median VCD values on top). The line represents the median difference. Box bounds represent 25 and 75 percentile, while whiskers indicate the 9 and 91 percentiles. The shaded area corresponds to the mission requirement of maximum 50% for the bias.

For the current work, 25 sites have contributed Pandora data, collected either from the ESA Atmospheric Validation Data Centre (EVDC) (<https://evdc.esa.int/>) or from the PGN data archive (<https://pandonia-global-network.org/>). Only data files from a recent quality upgrade (processor version 1.7, retrieval version nvs1, with file version 004 and 005; see <https://www.pandonia-global-network.org/home/documents/release-notes/>) were used, with 005 files (consolidated data) having precedence

over 004 files (rapid delivery data). The most important change with the previous data release is a more stringent quality filtering. Seventeen sites have provided measurement data newer than 3 months.

Except at low sun elevation, the footprint of these direct-sun measurements is much smaller than a TROPOMI pixel. Therefore, - as it is the case with MAX-DOAS - a significant horizontal smoothing difference error can be expected in the TROPOMI-
320 Pandora comparison, especially in the case of tropospheric NO₂ gradients and when tropospheric NO₂ is the largest contributor to the total column.

Three Pandora instruments (Alzomoni, Izaña, Mauna Loa) are located near the summit of a volcanic peak and are therefore not sensitive to the lower-lying tropospheric NO₂. In this work, their observations are compared to the TROPOMI stratospheric NO₂ data (see Sect. 3).

325 An important caveat must be formulated regarding the cross sections used in the data processing: As the scientific focus of the PGN up until processor version 1.7 (used for this study) was on measuring polluted conditions, i.e. in the presence of moderate to large tropospheric columns, the cross sections used in the processor are scaled to a fixed effective temperature of 254 K, which corresponds to the situation of approximately equal column amounts in the troposphere and stratosphere. As such the results are not entirely suited for observations in clean conditions where the column is dominated by the stratospheric
330 component (typical effective temperature of 220 K). In these background conditions, the PGN columns may be overestimated by up to 10%.

5.2 Filtering, co-location and harmonization

As was done for the tropospheric column validation in Sect. 4, only S5p pixels with qa_value at least 0.75 are retained. The so-called summed product is used, i.e. the total column computed as the stratospheric plus the tropospheric column values. This
335 summed column differs from the total column product. Only Pandonia measurements with the highest quality label (0 and 10) are used. The average column value within a 1-hour time interval, centered on the S5p overpass time, is used. As the NO/NO₂ ratio varies only slowly around the afternoon solar local time of the TROPOMI overpass, this small temporal window ensures no model-based adjustment is required. A 30-minute time interval was tested as well, but this did not change significantly the results. Moreover, only TROPOMI pixels containing the station were considered.

340 5.3 Comparison results

An example of a time series of co-located TROPOMI and PGN total column measurements, and their difference, is shown in Fig. 11.

Results for the entire PGN network are presented in Fig. 12. This figure reveals that the difference, even in relative units, depends strongly on the total NO₂ column, with low (or slightly positive) biases at low columns, and markedly negative biases
345 at high columns. No impact is observed for the TROPOMI ground pixel size switch of August 6, 2019.

Statistical estimators of the comparison results across the network are visualized in Fig. 13 and presented in tabular form in A3. One can distinguish roughly two different regimes.

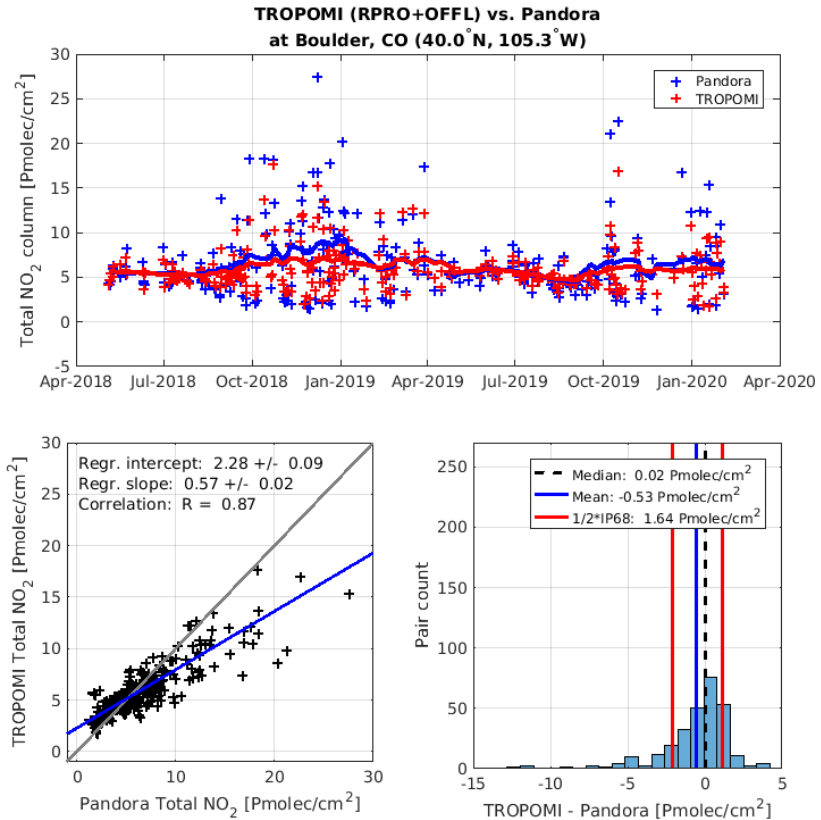


Figure 11. Same as Fig. 4 and Fig. 8, but now for the S5p OFFL total NO₂ column data co-located with ground-based Pandora measurements obtained at the PGN mid-latitude station of Boulder, Colorado.

(i) PGN median total column value between 3 (Alice Springs) and 6 Pmolec/cm² (New Brunswick). The absolute bias (median difference) is within ± 0.2 Pmolec/cm² in most cases (up to $+0.5$ Pmolec/cm² at Egbert and Helsinki) while the 350 median relative difference is within 5% in most cases (up to $\sim 10\%$ at Alice Springs, Egbert, Inoe and Helsinki). Canberra is a deviating case with larger negative bias (-0.9 Pmolec/cm²; -20%). The difference dispersion (IP68/2) roughly increases with increasing PGN NO₂ median VCD, from 0.4-0.6 Pmolec/cm² at the three cleanest sites, to 1-2 Pmolec/cm² at the other sites.

(ii) PGN NO₂ median total column value between 8 (Buenos Aires) and 19 Pmolec/cm² (UNAM, Mexico city). A negative bias is observed, ranging from -1 Pmolec/cm² (-15%) at The Bronx (New York) to -7 Pmolec/cm² (-50%) at Rome Sapienza. 355 The difference dispersion ranges from ~ 3 (Buenos Aires) to 5 Pmolec/cm² (UNAM).

The median relative difference is mostly within (or bordering) the $\pm 10\%$ range for the sites with lower NO₂ median total column values (Alice Springs to New Brunswick; Canberra is an exception), while it is negative and mostly outside this range, but still within $\pm 50\%$, for the sites with higher NO₂ median total column value (Buenos Aires to UNAM).

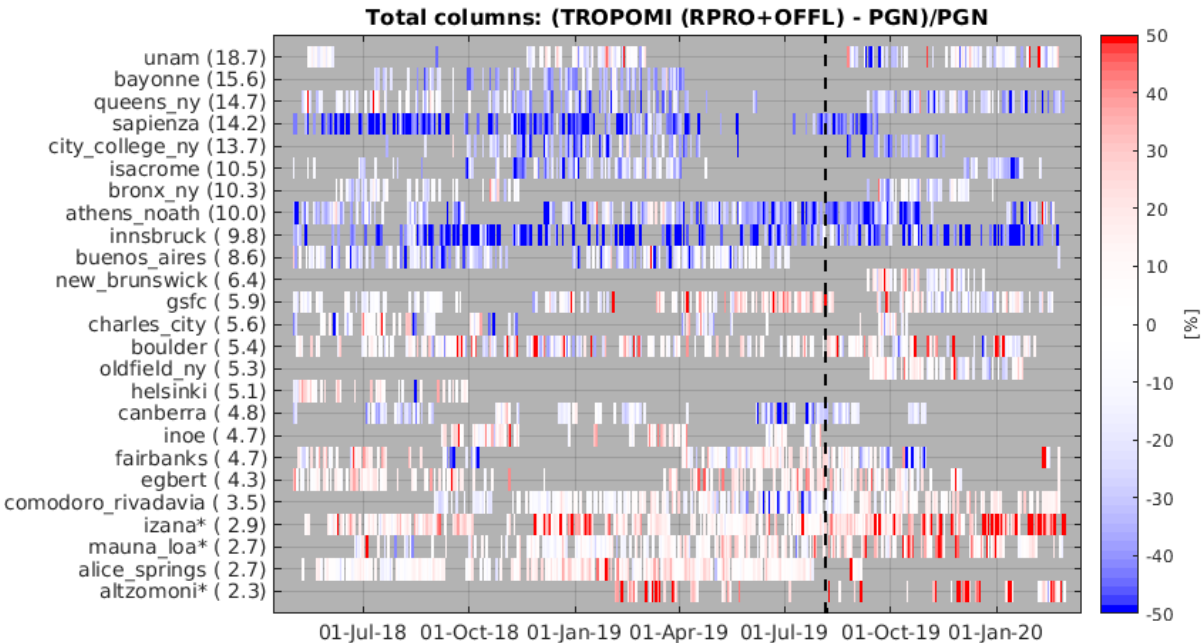


Figure 12. Percent relative difference between the S5p TROPOMI and PGN NO₂ total column data as a function of time. Stations are ordered by median NO₂ total column (lowest median value at the bottom). The dashed vertical line on August 6, 2019, represents the reduction in S5p ground pixel size from $7.0 \times 3.5 \text{ km}^2$ to $5.5 \times 3.5 \text{ km}^2$. The three mountain-top sites more suited for the validation of only the stratospheric column are marked with an asterisk.

The overall bias over all sites (median over all site medians or site relative medians) is -0.5 Pmolec/cm² (-7%). The overall dispersion is 1.8 Pmolec/cm² while the site-to-site dispersion (IP68/2 over all site medians) is 2.2 Pmolec/cm².
 360

It is however more useful to make the distinction between sites with low NO₂ (Alice Springs to New Brunswick) and high NO₂ (Buenos Aires to UNAM). For the low NO₂ sites, the overall bias is 0.1 Pmolec/cm² (2%), the overall dispersion is 1.1 Pmolec/cm² and the site-to-site dispersion is 0.2 Pmolec/cm². For the high NO₂ sites, the overall bias is -3.6 Pmolec/cm² (-32%), the overall dispersion is 3.3 Pmolec/cm² and the site-to-site dispersion is 1.4 Pmolec/cm².

365 6 Discussion and conclusions

A cross-networks summary of the median difference and dispersion for the three S5p NO₂ (sub)column data is attempted in Table 2. While the difference between the NRTI and OFFL NO₂ values can reach up to a few Pmolec/cm² for individual TROPOMI pixels, the two processing channels do not lead to significantly different validation results, and Table 2 therefore makes no distinction between the two.

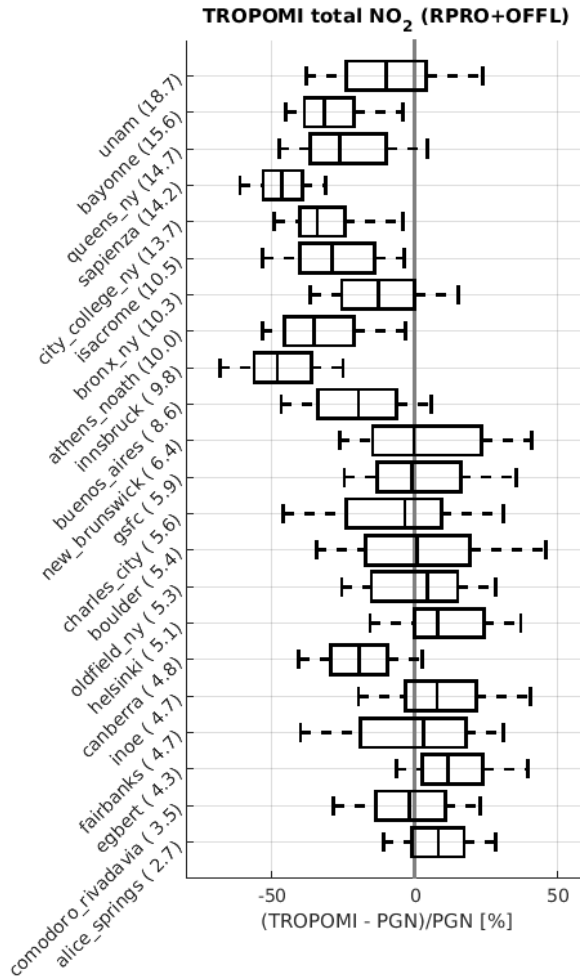


Figure 13. Same as Fig. 6 and Fig. 10, but now for the difference between S5p TROPOMI (RPRO+OFFL) and PGN NO₂ total columns. Stations are ordered by ground-based total NO₂ median value, like in Fig. 10. The median difference is represented by a vertical solid line inside the box, which marks the 25 and 75% quantiles. The whiskers cover the 9-91% range of the differences. The 3 mountain-top PGN instruments used for the validation of the stratospheric columns are not included here, but in Fig. 6.

370 For the stratospheric column, the general picture is a slight negative median difference of TROPOMI with respect to the NDACC ZSL-DOAS network, of the order of -0.2 Pmolec/cm² on average, with some station-to-station inhomogeneities and with larger differences in the highly variable conditions of the denoxified polar stratosphere in local winter. This median difference remains within the S5p mission requirements and is similar to the conclusions derived for similar satellite data from other sounders (e.g., Compernolle et al., 2020b). In view of the sources of systematic uncertainties in the different components

Table 2. Cross-networks summary of the validation results: bias (median) and dispersion (IP68/2) of the difference w.r.t the ground-based correlative measurements (median value over the stations).

	Bias	Dispersion
Stratosphere	-0.2 Pmolec cm^{-2} ; -9%	0.3 Pmolec/ cm^2
Troposphere		
low NO_2	-0.3 Pmolec cm^{-2} ; -23%	0.7 Pmolec cm^{-2}
high NO_2	-2 Pmolec cm^{-2} ; -37%	3.4 Pmolec cm^{-2}
extreme NO_2	-12 Pmolec cm^{-2} ; -51%	7 Pmolec cm^{-2}
Total column		
low NO_2	0.1 Pmolec cm^{-2} ; 2%	1 Pmolec cm^{-2}
high NO_2	-3.6 Pmolec cm^{-2} ; -30%	3 Pmolec cm^{-2}

375 of the comparison (satellite data, reference data, photochemical cycle adjustment, irreducible mismatch errors), this result is entirely within expectations. While comparisons to mountain-top PGN instruments confirms these values, using cross sections at a more appropriate (lower) temperature in the PGN data processing would lead to somewhat smaller columns and therefore a less significant negative median difference than that observed w.r.t. the ZSL-DOAS instruments. This probably reflects the true accuracy of the ground-based data, which should thus be taken to be of the order of $\pm 10\%$ at best.

380 For the tropospheric and total columns, averaging results over the networks with the hope to obtain a meaningful global estimate is of limited use as the results depend strongly on the amount of tropospheric NO_2 . Overall, mission requirements in terms of bias are mostly met, the only exception being the tropospheric columns at extremely polluted sites, which have a bias on the threshold of 50%. Nevertheless, it is clear that large negative median differences are observed across all sites experiencing significant tropospheric pollution. The dispersion of the difference is well outside of the mission requirements 385 formulated for the tropospheric column data. Nevertheless, these results are consistent with those obtained with completely different validation techniques, such as explored by Lorente et al. (2019) over Paris (using ground-based and Eiffel Tower NO_2 concentrations and a climatology of observed column-to-surface ratios). Many factors play a role in this apparent disagreement between TROPOMI and the ground-based networks, that can neither be attributed solely to the S5p data, nor to pure area-averaging differences.

390 First: Local horizontal and vertical variations of the NO_2 field can explain (part of) such discrepancies, as illustrated in Chen et al. (2009); Pinardi et al. (2020); Compernolle et al. (2020b); Dimitropoulou et al. (2020). While the MAX-DOAS picks up small local enhancements, the much larger satellite pixel provides a smoothed perception of the field. In particular for sounders with footprints (much) larger than the emission sources, this generally leads to under-estimation in urban conditions while having better agreement in remote locations (Celarier et al., 2008; Kanaya et al., 2014; Pinardi et al., 2020). Dimitropoulou 395 et al. (2020) showed specific improvements of the S5p NO_2 comparison results in the case of the Uccle MAX-DOAS when making use of the multiple azimuthal scan mode and when improving the S5p selection criteria to pixels along the MAX-DOAS field of view direction and within the effective sensitivity length. Large inhomogeneities around MAX-DOAS sites

were also shown by (Wang et al., 2014; Ortega et al., 2015; Gratsea et al., 2016; Peters et al., 2019; Schreier et al., 2020). When taking part of these inhomogeneities into account in validation of other sounders, results had been improved (Brinksma 400 et al., 2008). Judd et al. (2019) also showed the smoothing of the NO₂ field when re-sampling GeoTASO high-resolution airborne measurements to different simulated satellite pixel sizes.

Second: Vertical sensitivity (and thus averaging kernels) and a priori vertical profiles are known to be different for MAX-DOAS and nadir UV-visible satellite retrievals (Wang et al., 2017; Liu et al., 2019b; Compernolle et al., 2020b), with MAX-DOAS measurements sensitive to layers close to the surface and satellite retrievals sensitive mostly to the free troposphere. The 405 effect of the a-priori vertical profile on the comparison was estimated for TROPOMI by Dimitropoulou et al. (2020) for Uccle, showing an increase by about 55% when recalculating the TROPOMI column with MAX-DOAS daily mean tropospheric profile. Similarly, Ialongo et al. (2020) and Zhao et al. (2019) show improvement of the agreement between TROPOMI and Pandora total column data for episodes of NO₂ enhancement, when replacing the coarse a-priori NO₂ profiles with high-resolution profiles from a high-resolution regional air quality forecast model. Somewhat related to the vertical sensitivity is 410 the treatment of aerosol optical depth and its vertical profile. Poor representation of the aerosol opacity has been shown (from simulations) to cause both underestimated NO₂ in satellite retrievals and overestimated NO₂ in MAX-DOAS measurements (Leitão et al., 2010; Ma et al., 2013; Jin et al., 2016). Satellite-ground discrepancies in previous validation studies have already been attributed to such aerosol issues (Boersma et al., 2018; Compernolle et al., 2020b). Moreover, explicit aerosol corrections in the S5p retrievals have already been shown to improve the agreement (Liu et al., 2020).

415 Third: The treatment of cloud properties can have a significant effect on the retrieval of the TROPOMI NO₂ tropospheric VCD. Eskes et al. (2020) discuss the comparison with OMI NO₂ tropospheric column retrievals and show that on an average TROPOMI is lower than OMI by -10% to -12% over Europe, North America and India, and up to -22% over China. This difference is mainly attributed to the different cloud data product used in the NO₂ retrieval: FRESCO-S derives the cloud 420 top pressure from TROPOMI radiances in the near-infrared O₂-A band, while for OMI the cloud top pressure is retrieved from the O₂-O₂ band in the UV-Visible. Preliminary validation results (Compernolle et al., 2020a, and H. Eskes, private communication) indicate that FRESCO-S is biased high in pressure, especially at altitudes close to the surface. A new version of FRESCO-S with an adapted wavelength window has been implemented and seems to remove most of the 10-22% bias with OMI in polluted regions.

425 Fourth: Although this work, Compernolle et al. (2020b), and Pinardi et al. (2020) all show a generally good coherence of the validation results among the MAX-DOAS instruments across the network and also among MAX-DOAS and Pandora instruments, network homogenization remains an important challenge to focus on to improve the accuracy of future satellite validations (see Sect. 4 for a description of contributors to network in-homogeneity). Inter-comparison campaigns, such as the CINDI-1 and -2 (Piters et al., 2012; Kreher et al., 2019), in-depth intercomparison studies of the retrieval methods (Frieß et al., 2019; Tirpitz et al., 2020; Peters et al., 2019), and dedicated projects aiming at the harmonization of the processing and 430 of the associated metadata (such as the FRM4DOAS project of ESA's Fiducial Reference Measurements programme) are an important way to achieve this.

Regarding the mutual consistency of MAX-DOAS and PGN based validation results: while it may appear that, at low column values, PGN base comparisons indicate a smaller bias than the MAX-DOAS comparisons, one must not forget that PGN measures the total column: at stations with a lower total column value, the stratospheric contribution is relatively more important. The better agreement here is therefore consistent with the good agreement found for the TROPOMI stratospheric NO₂ column vs. ZSL-DOAS and also vs. PGN at pristine mountain sites (Section 3). For sites characterised by a higher total NO₂ column, the tropospheric contribution becomes more important, and some of the same effects that make satellite-to-MAX-DOAS comparisons difficult, such as smoothing difference error, lower sensitivity of the satellite close to the surface, and approximate S5p a-priori profile, come into play as well.

In conclusion, the first two years of Copernicus S5p TROPOMI NO₂ column data produced both with the NRTI and OFFL versions 01.0x.xx of the operational processors, do meet mission requirements for the bias, and to some extent and with precaution for the uncertainty (dispersion). The different data products available publicly through the Copernicus system are mutually consistent, in good geophysical and quantitative agreement with ground-based correlative data of documented quality, and can be used for a variety of applications, on the condition that the features and limitations exposed here are taken into proper consideration, and that the S5p data are filtered and used according to the recommendations provided in the official Product Readme File (PRF) and associated documentation, also available publicly. Ground-based validation activities relying on the correlative measurements contributed by the NDACC ZSL-DOAS, MAX-DOAS and PGN global monitoring networks, have progressed significantly in recent years and have demonstrated their capacity, but also their current limitations in an operational context such as the Copernicus programme. Room does exist for further improvement of both the satellite and ground-based data sets, as well as the intercomparison methodology and its associated error budget. Beyond the methodology advances published here and in aforementioned papers, special effort is needed to understand fully and ever reduce comparison mismatch errors, which so far make difficult the accurate validation of S5p data uncertainty bars. Several updates of the calibration of TROPOMI spectra and of the TROPOMI NO₂ data retrieval processors are already in development and in implementation. Upcoming data versions should be validated with the same system as used in the current paper, allowing the necessary independent assessment of the S5p data product evolution.

Appendix A: Ground networks

A1 The NDACC ZSL-DOAS network

Table A1. ZSL-DOAS hosting stations, ordered by latitude, that are contributing to the stratospheric NO_2 column validation. Several measures of the agreement between TROPOMI and the ground-based data are also provided. The bias over all stations (median over all station median differences) is $-0.23 \text{ Pmolec cm}^{-2}$ while the overall dispersion (median over all 1/2IP68) is $0.31 \text{ Pmolec cm}^{-2}$ and the inter-station dispersion (1/2IP68 over all station medians) is $0.30 \text{ Pmolec cm}^{-2}$.

Station	Latitude	Longitude	Altitude	Institute	Processing	Median diff.	Spread (1P68/2)	R
	[deg]	[deg]	[m] a.m.s.l.			[Pmolec/cm ²]	[Pmolec/cm ²]	
Eureka	80.05	-86.42	610	U. Toronto	NDACC	0.04 = 1%	0.60	0.89
Eureka	80.05	-85.42	610	LATMOS-CNRS + U. Toronto	LATMOS_RT	-0.00 = 0%	0.20	0.97
Ny-Ålesund	78.92	11.93	10	NILU	LATMOS_RT	-0.93 = -26%	0.24	0.97
Scoresbysund	70.48	-21.95	67	LATMOS-CNRS + DMI	LATMOS_RT	-0.16 = -5%	0.32	0.98
Sodankylä	67.37	26.63	179	LATMOS-CNRS + FMI	LATMOS_RT	-0.42 = -12%	0.37	0.97
Harestua	60.00	10.75	596	BIRA-IASB	NDACC	-0.18 = -6%	0.36	0.95
Zvenigorod	55.69	36.77	220	IAP, RAS	NDACC	-0.04 = -2%	0.67	0.69
Bremen	53.10	8.85	27	IUP Bremen	NDACC	-0.60 = -19%	0.40	0.91
Paris	48.85	2.35	63	LATMOS-CNRS	LATMOS_RT	-0.50 = -16%	0.56	0.59
Guyancourt	48.78	2.03	160	LATMOS-CNRS	LATMOS_RT	-0.40 = -13%	0.45	0.71
Haute Provence (O.H.P.)	43.94	5.71	650	LATMOS-CNRS	LATMOS_RT	-0.23 = -8%	0.23	0.94
Issyk-Kul	42.62	76.99	1640	KNU	NDACC	-0.33 = -9%	0.19	0.48
Athens	38.05	23.86	527	IUP Bremen + NOA	NDACC	-0.02 = -1%	0.28	0.89
Izaña	28.31	-16.50	2367	INTA	NDACC	-0.10 = -4%	0.14	0.95
Saint-Denis	-20.90	55.48	110	LATMOS-CNRS + LACY	LATMOS_RT	0.05 = 2%	0.18	0.80
Bauru	-22.35	-49.03	640	LATMOS-CNRS + UNESP	LATMOS_RT	-0.31 = -12%	0.19	0.80
Lauder	-45.04	169.68	370	NIWA	NDACC	-0.77 = -23%	0.28	0.92
Kerguelen	-49.35	70.26	36	LATMOS-CNRS	LATMOS_RT	-0.21 = -7%	0.34	0.94
Rio Gallegos	-51.60	-69.32	15	LATMOS-CNRS	LATMOS_RT	-0.45 = -16%	0.28	0.95
Macquarie	-54.50	158.94	6	NIWA	NDACC	-1.01 = -27%	0.48	0.93
Ushuaia	-54.82	-68.32	7	INTA	NDACC	0.09 = 4%	0.40	0.95
Marambio	-64.23	-56.72	198	INTA	NDACC	0.09 = 3%	0.39	0.97
Dumont d'Urville	-66.67	140.02	45	LATMOS-CNRS	LATMOS_RT	0.20 = 5%	0.50	0.95
Neumayer	-70.63	-8.25	43	U. Heidelberg	NDACC	-0.06 = -5%	0.21	0.95
Dome Concorde	-75.10	123.31	3250	LATMOS-CNRS	LATMOS_RT	-0.16 = -6%	0.38	0.95
Arrival Heights	-77.83	166.66	184	NIWA	NDACC	-0.52 = -26%	0.25	0.90

A2 The MAX-DOAS network

Table A2. MAX-DOAS hosting stations, ordered by increasing median tropospheric column (VCDgb, lowest at the bottom), that are contributing to the tropospheric NO₂ column validation. More details on the QA4ECV data sets can be found at <http://www.qa4ecv.eu/ecvs>. References are the following: [a] Arellano et al. (2016), [b] Friedrich et al. (2019), [c] Xing et al. (2020), [d] Xing et al. (2017), [e] Hendrick et al. (2014), [f] Irie et al. (2011), [g] Irie et al. (2012), [h] Irie et al. (2015), [i] Kanaya et al. (2014), [j] Vlemmix et al. (2010), [k] Gielen et al. (2014), [l] Hoque et al. (2018), [m] Drosoglou et al. (2017). Several measures of the agreement between TROPOMI and the ground-based data are also provided. Biases and comparison spreads vary strongly between stations, mainly as a function of the nature of the site (clean or polluted). When calculating these numbers for the three regimes (clean, polluted, extreme), the median biases are: -0.3, -2 and -12 Pmolec/cm² (-23%, -37% and -51%) respectively, with median dispersions of: 0.7, 3.4 and 7 Pmolec/cm². Note that the median values for the high tropospheric columns (Athens to Xianghe) are almost the same as the statistics found for the whole network. The site-to-site bias dispersion is 0.2, 1.2 and 3.3 Pmolec/cm² for each regime.

Station	Latitude	Longitude	Altitude	Institute	Retrieval and Format	Reference med(VCDgb)	Med(diff)	Spread (IP68/2)	R	
	[deg]	[deg]	m a.m.s.l.	Type	[Pmolec/cm ²]	[Pmolec/cm ² , %]	[Pmolec/cm ²]			
Vallejo	19.48	-99.15	2255	UNAM	OE (MMF), GEOMS	[a,b]	29	-14; -51.3%	12	0.40
UNAM	19.33	-99.18	2280	UNAM	OE (MMF), GEOMS	[a,b]	19	-7.8; -37.3%	7	0.84
Cuauitlan	19.72	-99.20	2263	UNAM	OE (MMF), GEOMS	[a,b]	17	-12; -73.8%	4.3	0.70
Gucheng	39.15	115.73	13.4	USTC	GA, ascii	[c,d]	14	-5.4; -35.3%	6.5	0.86
Xianghe	39.75	116.96	95	BIRA-IASB	OE (bePRO), GEOMS	[e]	11	-3.9; -31.7%	5.7	0.83
Chiba	35.60	140.10	21	ChibaU	PP, ascii	[f,g,h]	8.6	-1; -15%	6.3	0.79
Yokosuka	35.32	139.65	10	JAMSTEC	PP, GEOMS	[i]	8.1	-2.4; -33%	3.7	0.85
Kasuga	33.52	130.48	28	ChibaU	PP, ascii	[f,g,h]	7.3	-3.1; -50.4%	4	0.46
Mainz	49.99	8.23	150	MPIC	QA4ECV dataset, GEOMS		7.3	-3.3; -41%	3.3	0.75
Cabauw	51.97	4.93	3	KNMI	PP, GEOMS	[j]	6.7	-2.5; -36.5%	3.5	0.40
Uccle	50.80	4.36	120	BIRA-IASB	OE (bePRO), GEOMS	[k]	5.7	-2.3; -37%	3.3	0.75
De Bilt	52.10	5.18	20	KNMI	PP, GEOMS	[j]	5.4	-0.95; -16.8%	2.8	0.64
Bremen	53.10	8.85	27	IUPB	QA4ECV dataset, GEOMS		5.2	-2.1; -37%	2.3	0.59
Pantnagar	29.03	79.47	237	ChibaU	PP, ascii	[f,g,h,l]	4.6	-2.6; -56%	1.6	0.33
Thessaloniki_lap	40.63	22.96	60	AUTH	QA4ECV dataset, GEOMS	[m]	4.6	-1.5; -43.8%	4.1	0.69
Thessaloniki_ciri	40.56	22.99	70	AUTH	QA4ECV dataset, GEOMS	[m]	3.6	-1.3; -34.9%	2	0.73
Athens	38.05	23.86	527	IUPB	QA4ECV dataset, GEOMS		3.4	-1.1; -36.7%	3	0.66
Phimai	15.18	102.56	212	ChibaU	PP, ascii	[f,g,h,l]	2	-0.5; -26.6%	0.7	0.47
Fukue	32.75	128.68	80	JAMSTEC	PP, GEOMS	[i]	0.95	-0.18; -18.5%	0.6	0.01

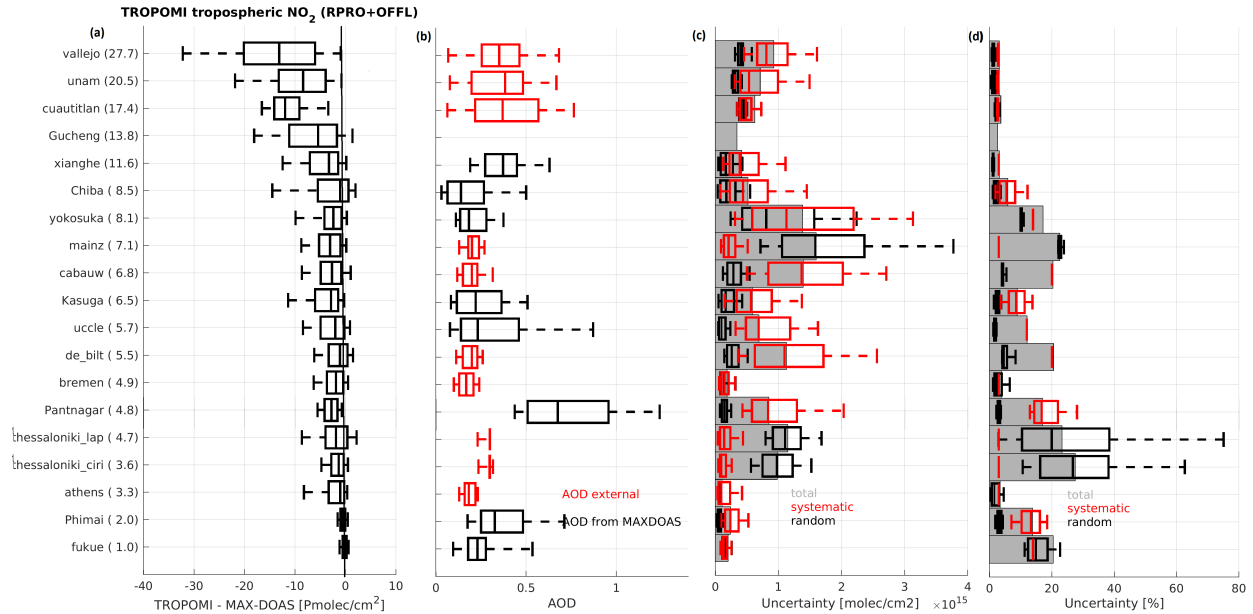


Figure A1. (a) Box-and-whisker plots summarizing the TROPOMI - MAX-DOAS tropospheric VCD difference, per station, ordered as a function of the median ground-based tropospheric column (largest median VCD values on top). (b), (c) and (d) present, respectively, the assumed aerosol optical depth (AOD, either retrieved from the MAX-DOAS measurement or taken from the climatology used in the NO₂ retrieval), the MAX-DOAS absolute uncertainties, and the relative uncertainties (total median uncertainty in grey bars, random part in black and systematic part in red).

A3 The Pandonia Global Network

Table A3. PGN stations, ordered by median PGN NO₂ column value, that are contributing to the total NO₂ validation. Mountain-top stations (not sensitive to lower lying tropospheric NO₂) are marked with an asterisk. In the last row, we indicated where the data can be obtained (EVDC or directly from the PGN website). Note that only PGN data from a recent quality upgrade (with file version 004 or 005, where 005 has precedence) was used. The bias over all stations (median over all station medians) is -0.5 Pmoleccm⁻² (-7%) while the overall dispersion (median over all 1/2IP68) is 1.8 Pmoleccm⁻² and the inter-station dispersion (1/2IP68 over all station medians) is 2.2 Pmoleccm⁻². Considering the low NO₂ stations (Alice Springs to New Brunswick) only, the bias is 0.1 Pmoleccm⁻² (2%), the overall dispersion is 1.1 Pmoleccm⁻² and the inter-station dispersion is 0.2 Pmoleccm⁻². For the high NO₂ stations (Buenos Aires to UNAM), the bias is -3.6 Pmoleccm⁻² (-30%), the overall dispersion is 3.3 Pmoleccm⁻² and the inter-station dispersion is 1.4 Pmoleccm⁻². Note that the mountain-top stations are not used in the calculation of these overall statistics.

Station code	Full name	Lat [°]	Lon [°]	Alt [m]	PGN med(VCD)	med(diff) ;med(rediff)	1/2IP68(diff)	R [Pmoleccm ⁻²]	R [Pmoleccm ⁻²]	R archive
unam	National Autonomous University of Mexico	19.33	-99.18	2280	18.7	-2.1;-10%	-2.1;-10%	4.6	0.87	both
Bayonne	Bayonne	40.67	-74.13	3	15.6	-4.3;-31%	-4.3;-31%	3.2	0.88	EVDC
queens_ny	New York Queens College	40.74	-73.82	25	14.7	-3.7;-26%	-3.7;-26%	3.6	0.84	EVDC
sapienza	Rome Sapienza	41.90	12.52	75	14.2	-6.6;-46%	-6.6;-46%	4.0	0.81	EVDC
city_college_ny	New York City College	40.82	-73.95	113	13.7	-4.7;-34%	-4.7;-34%	3.4	0.91	EVDC
isacrome	Rome CNR-ISAC	41.84	12.65	117	10.5	-2.7;-29%	-2.7;-29%	3.2	0.85	both
bronx_ny	New York - The Bronx	40.87	-73.88	31	10.3	-1.0;-13%	-1.0;-13%	3.3	0.90	both
athens_noath	Athens National Observatory	37.99	23.77	130	10.0	-3.4;-35%	-3.4;-35%	2.8	0.70	PGN
innsbruck	Innsbruck	47.26	11.39	616	9.8	-4.7;-48%	-4.7;-48%	3.4	0.59	PGN
buenos_aires	Buenos Aires	-34.56	-58.51	20	8.6	-1.8;-20%	-1.8;-20%	2.6	0.86	both
new_brunswick	New Brunswick (NJ)	40.46	-74.43	19	6.4	-0.0;-0%	-0.0;-0%	1.5	0.90	PGN
gsfc	Goddard Space Flight Center	38.99	-76.84	90	5.9	-0.1;-1%	-0.1;-1%	1.3	0.80	both
charles_city	Charles City (VA)	37.33	-77.21	6	5.6	-0.2;-3%	-0.2;-3%	2.0	0.44	both
boulder	Boulder	39.99	-105.26	1660	5.4	0.0;1%	0.0;1%	1.6	0.87	both
oldfield_ny	New York - Old Field	40.96	-73.14	3	5.3	0.2;5%	0.2;5%	1.1	0.93	both
helsinki	Helsinki	60.20	24.96	97	5.1	0.5;8%	0.5;8%	1.0	0.77	EVDC
canberra	Canberra	-35.34	149.16	600	4.8	-0.9;-19%	-0.9;-19%	0.9	0.64	EVDC
inoe	Magurele	44.34	26.01	93	4.7	0.3;8%	0.3;8%	1.0	0.79	EVDC
fairbanks	Fairbanks	64.86	-147.85	227	4.7	0.1;3%	0.1;3%	1.4	0.43	EVDC
egbert	Egbert	44.23	-79.78	251	4.3	0.5;12%	0.5;12%	0.6	0.88	PGN
comodoro_rivadavia	Comodoro Rivadavia	-45.78	-67.45	46	3.5	-0.1;-2%	-0.1;-2%	0.6	0.56	PGN
izana*	Izana	28.31	-16.50	2360	2.9	0.6;19%	0.6;19%	0.5	0.53	both
mauna_loa*	Mauna Loa	19.48	-155.60	4169	2.7	0.2;6%	0.2;6%	0.5	0.43	both
alice_springs	Alice Springs	-23.76	133.88	567	2.7	0.2;8%	0.2;8%	0.4	0.61	EVDC
altzomoni*	Altzomoni	19.12	-98.66	3985	2.3	0.7;28%	0.7;28%	0.6	0.64	both

460 *Author contributions.* TV, SC and GP carried out the global validation analysis. JCL, KUE and MVR contributed input and advise at all stages of the analysis. AMF (EVDC), JG (Multi-TASTE) and SN (MPC VDAF-AVS) pre- and/or post-processed the ground-based and satellite data. HJE, KFB, PFL and JPV developed the TROPOMI NO₂ data processor. AR, MVR and TW contributed expertise on satellite NO₂ data retrieval. AC, FH, KK, MT, APa, JPP and MVR supervise networks operation and contributed ground-based scientific expertise. AD, LSdM and CZ supervise the Copernicus S5p mission, the S5p MPC and the S5PVT. All other co-authors contributed ground-based data 465 and expertise at ground-based stations. TV, SC, GP and JCL wrote and edited the manuscript. All co-authors revised and commented on the manuscript.

Competing interests. The authors declare that they have no conflict of interest.

470 *Acknowledgements.* Part of the reported work was carried out in the framework of the Copernicus Sentinel-5 Precursor Mission Performance Centre (S5p MPC), contracted by the European Space Agency (ESA/ESRIN, Contract No. 4000117151/16/I-LG) and supported by the Belgian Federal Science Policy Office (BELSPO), the Royal Belgian Institute for Space Aeronomy (BIRA-IASB), the Netherlands Space Office (NSO), and the German Aerospace Centre (DLR). Part of this work was carried out also in the framework of the S5p Validation Team (S5PVT) AO projects NIDFORVAL (ID #28607, PI G. Pinardi, BIRA-IASB) and CESAR (ID #28596, PI A. Apituley, KNMI). S. Compernolle, G. Pinardi and T. Verhoelst at BIRA-IASB acknowledge national funding from BELSPO and ESA through the ProDEX projects TROVA-E2 (PEA 4000116692). The authors express special thanks to A.M. Fjæraa, J. Granville, S. Niemeijer and O. Rasson for 475 post-processing of the network and satellite data and for their dedication to the S5p operational validation.

480 This work contains modified Copernicus Sentinel-5 Precursor satellite data (2018-2020) processed by KNMI and post-processed by BIRA-IASB. The ZSL-DOAS and Pandora data used in this publication were obtained as part of the Network for the Detection of Atmospheric Composition Change (NDACC, <https://ndacc.org>) and the Pandonia Global Network (PGN, <https://www.pandonia-global-network.org/>), respectively, and are publicly available. The LATMOS Real-Time processing facility is acknowledged for fast delivery of ZSL-DOAS SAOZ data. Fast delivery of MAX-DOAS data tailored to the S5p validation was organized through the S5PVT AO project NIDFORVAL. The authors are grateful to ESA/ESRIN for supporting the ESA Validation Data Centre (EVDC) established at NILU, and for running the Fiducial Reference Measurements (FRM) programme and in particular the FRM4DOAS and Pandonia projects. The PGN is a bilateral project between NASA and ESA, and the NASA funding for the PGN is provided through the NASA Tropospheric Composition Program and Goddard Space Flight Center Pandora project.

485 The MAX-DOAS, ZSL-DOAS and PGN instrument PIs and staff at the stations are thanked warmly for their sustained effort on maintaining high quality measurements and for valuable scientific discussions. A. Elokhov and A. Gruzdev acknowledge national funding from RFBR through the project 20-05-274. IUP-Bremen acknowledges DLR-Bonn for funding received through project 50EE1709A. The SAOZ network acknowledges funding from the French Institut National des Sciences de l'Univers (INSU) of the Centre National de la Recherche Scientifique (CNRS), Centre National d'Etudes Spatiales (CNES) and Institut polaire français Paul Emile Victor (IPEV). Work done by HII 490 was supported by the Environment Research and Technology Development Fund (2-1901) of the Environmental Restoration and Conservation Agency of Japan, JSPS KAKENHI (grant numbers JP19H04235 and JP17K00529), the JAXA 2nd research announcement on the Earth Observations (grant number 19RT000351), and JST CREST (grant number JPMJCR15K4). The U Toronto ZSL-DOAS measurements at Eureka were made at the Polar Environment Atmospheric Research Laboratory (PEARL) by the Canadian Network for the Detection of

Atmospheric Change (CANDAC), with support from the Canadian Space Agency (AVATARS project), the Natural Sciences and Engineering
495 Research Council (PAHA project), and Environment and Climate Change Canada.

References

Arellano, J., Krüger, A., Rivera, C., Stremme, W., Friedrich, M., Bezanilla, A., and Grutter, M.: The MAX-DOAS network in Mexico City to measure atmospheric pollutants, *Atmosfera*, 29, 157–167, <https://doi.org/10.20937/ATM.2016.29.02.05>, <http://www.revistascca.unam.mx/atm/index.php/atm/article/view/ATM.2016.29.02.05>, 2016.

500 Beirle, S., Dörner, S., Donner, S., Remmers, J., Wang, Y., and Wagner, T.: The Mainz profile algorithm (MAPA), *Atmospheric Measurement Techniques*, 12, 1785–1806, <https://doi.org/10.5194/amt-12-1785-2019>, <https://www.atmos-meas-tech.net/12/1785/2019/>, 2019.

Blechschmidt, A.-M., Arteta, J., Coman, A., Curier, L., Eskes, H., Foret, G., Gielen, C., Hendrick, F., Marécal, V., Meleux, F., Parmentier, J., Peters, E., Pinardi, G., Piters, A. J. M., Plu, M., Richter, A., Sofiev, M., Valdebenito, Á. M., Van Roozendael, M., Vira, J., Vlemmix, T., and Burrows, J. P.: Comparison of tropospheric NO₂ columns from MAX-DOAS retrievals and regional air quality model simulations, *Atmospheric Chemistry and Physics*, pp. 2795–2823, <https://doi.org/10.5194/acp-2016-1003>, 2020.

Boersma, K. F., Eskes, H. J., Veefkind, J. P., Brinksma, E. J., van der A, R. J., Sneep, M., van den Oord, G. H. J., Levelt, P. F., Stammes, P., Gleason, J. F., and et al.: Near-real time retrieval of tropospheric NO₂ from OMI, *Atmos. Chem. Phys.*, 7, 2103–2118, <https://doi.org/10.5194/acp-7-2103-2007>, 2007.

Boersma, K. F., Eskes, H. J., Dirksen, R. J., van der A, R. J., Veefkind, J. P., Stammes, P., Huijnen, V., Kleipool, Q. L., Sneep, M., Claas, J., 510 Leitão, J., Richter, A., Zhou, Y., and Brunner, D.: An improved tropospheric NO₂ column retrieval algorithm for the Ozone Monitoring Instrument, *Atmos. Meas. Tech.*, 4, 1905–1928, <https://doi.org/10.5194/amt-4-1905-2011>, 2011.

Boersma, K. F., Eskes, H. J., Richter, A., De Smedt, I., Lorente, A., Beirle, S., van Geffen, J. H. G. M., Zara, M., Peters, E., Van Roozendael, M., Wagner, T., Maasakers, J. D., van der A, R. J., Nightingale, J., De Rudder, A., Irie, H., Pinardi, G., Lambert, J.-C., and Compernolle, S. C.: Improving algorithms and uncertainty estimates for satellite NO₂ retrievals: results from the quality assurance for the essential 515 climate variables (QA4ECV) project, *Atmospheric Measurement Techniques*, 11, 6651–6678, <https://doi.org/10.5194/amt-11-6651-2018>, <https://www.atmos-meas-tech.net/11/6651/2018/>, 2018.

Bognar, K., Zhao, X., Strong, K., Boone, C., Bourassa, A., Degenstein, D., Drummond, J., Duff, A., Goutail, F., Griffin, D., Jeffery, P., Lutsch, E., Manney, G., McElroy, C., McLinden, C., Millán, L., Pazmino, A., Sioris, C., Walker, K., and Zou, J.: Updated validation of ACE and OSIRIS ozone and NO₂ measurements in the Arctic using ground-based instruments at Eureka, Canada, *Journal of Quantitative 520 Spectroscopy and Radiative Transfer*, 238, 106 571, <https://doi.org/https://doi.org/10.1016/j.jqsrt.2019.07.014>, 2019.

Bösch, T., Rozanov, V., Richter, A., Peters, E., Rozanov, A., Wittrock, F., Merlaud, A., Lampel, J., Schmitt, S., de Hajj, M., Berkhouit, S., Henzing, B., Apituley, A., den Hoed, M., Vonk, J., Tiefengraber, M., Müller, M., and Burrows, J. P.: BOREAS – a new MAX-DOAS profile retrieval algorithm for aerosols and trace gases, *Atmospheric Measurement Techniques*, 11, 6833–6859, <https://doi.org/10.5194/amt-11-6833-2018>, <https://www.atmos-meas-tech.net/11/6833/2018/>, 2018.

525 Bovensmann, H., Burrows, J. P., Buchwitz, M., Frerick, J., Noël, S., Rozanov, V. V., Chance, K. V., and Goede, A. P. H.: SCIAMACHY: Mission Objectives and Measurement Modes, *Journal of the Atmospheric Sciences*, 56, 127–150, 1999.

Brinksma, E. J., Pinardi, G., Volten, H., Braak, R., Richter, A., Scho, A., Van Roozendael, M., Fayt, C., Hermans, C., Dirksen, R. J., Vlemmix, T., Berkhouit, A. J. C., Swart, D. P. J., Oetjen, H., Wittrock, F., Wagner, T., Ibrahim, O. W., Leeuw, G. D., Moerman, M., Curier, R. L., Celarier, E. A., Cede, A., Knap, W. H., Veefkind, J. P., Eskes, H. J., Allaart, M., Rothe, R., Piters, A., and Levelt, P. F.: The 2005 and 2006 DANDELIONS NO₂ and aerosol intercomparison campaigns, *Journal of Geophysical Research*, 113, 1–18, <https://doi.org/10.1029/2007JD008808>, <http://www.agu.org/pubs/crossref/2008/2007JD008808.shtml>, 2008.

Burrows, J. P., Weber, M., Buchwitz, M., Rozanov, V., Ladstätter-Weißenmayer, A., Richter, A., DeBeek, R., Hoogen, R., Bramstedt, K., Eichmann, K.-U., Eisinger, M., and Perner, D.: The Global Ozone Monitoring Experiment (GOME): Mission Concept and First Scientific Results, *Journal of the Atmospheric Sciences*, 56, 151–175, 1999.

535 Celarier, E. A., Brinksma, E. J., Gleason, J. F., Veefkind, J. P., Cede, A., Herman, J. R., Ionov, D., Pommereau, J.-P., Goutail, F., Lambert, J.-C., Pinardi, G., Van Roozendael, M., Wittrock, F., Schonhardt, A., Richter, A., Ibrahim, O. W., Wagner, T., Bojkov, B., Mount, G., Spine, E., Chen, C. M., Pongett, T. J., Sander, S. P., Bucsela, E. J., O.Wenig, M., Swart, D. P. J., Volten, H., Levelt, P. F., and Kroon, M.: Validation of Ozone Monitoring Instrument nitrogen dioxide columns, *Journal of Geophysical Research*, 113, <https://doi.org/10.1029/2007JD008908>, 2008.

540 Chen, D., Zhou, B., Beirle, S., Chen, L. M., and Wagner, T.: Tropospheric NO₂ column densities deduced from zenith-sky DOAS measurements in Shanghai, China, and their application to satellite validation, *Atmospheric Chemistry and Physics*, 9, 3641–3662, <https://doi.org/10.5194/acp-9-3641-2009>, <https://www.atmos-chem-phys.net/9/3641/2009/>, 2009.

545 Choi, S., Lamsal, L. N., Follette-Cook, M., Joiner, J., Krotkov, N. A., Swartz, W. H., Pickering, K. E., Loughner, C. P., Appel, W., Pfister, G., Saide, P. E., Cohen, R. C., Weinheimer, A. J., and Herman, J. R.: Assessment of NO₂ observations during DISCOVER-AQ and KORUS-AQ field campaigns, *Atmos. Meas. Tech. Discuss.*, 2019, 1–43, <https://doi.org/10.5194/amt-2019-338>, 2019.

Clémér, K., Van Roozendael, M., Fayt, C., Hendrick, F., Hermans, C., Pinardi, G., Spurr, R., Wang, P., and De Mazière, M.: Multiple wavelength retrieval of tropospheric aerosol optical properties from MAXDOAS measurements in Beijing, *Atmospheric Measurement Techniques*, 3, 863–878, <https://doi.org/10.5194/amt-3-863-2010>, <http://www.atmos-meas-tech.net/3/863/2010/>, 2010.

550 Compernolle, S., Argyrouli, A., Lutz, R., Sneep, M., Lambert, J.-C., Fjæraa, A., Hubert, D., Keppens, A., Loyola, D., O'Connor, E., Romahn, F., Stammes, P., Verhoelst, T., and P., W.: Validation of the Sentinel-5 Precursor TROPOMI cloud data with Cloudnet, Aura OMI O₂-O₂ and Suomi-NPP VIIRS, in preparation for Atmospheric Measurement Techniques, April 2020, 2020a.

Compernolle, S., Verhoelst, T., Pinardi, G., Granville, J., Hubert, D., Keppens, A., Niemeijer, S., Rino, B., Bais, A., Beirle, S., Boersma, F., Burrows, J. P., De Smedt, I., Eskes, H., Goutail, F., Hendrick, F., Lorente, A., Pazmino, A., Piters, A., Peters, E., Pommereau, J.-P., Remmers, J., Richter, A., van Geffen, J., Van Roozendael, M., Wagner, T., and Lambert, J.-C.: Validation of Aura-OMI QA4ECV NO₂ Climate Data Records with ground-based DOAS networks: role of measurement and comparison uncertainties, *Atmos. Chem. Phys. Discuss.*, 2020, 1–44, <https://doi.org/10.5194/acp-2019-877>, 2020b.

555 De Mazière, M., Thompson, A., Kurylo, M., Wild, J., Bernhard, G., Blumenstock, T., Braathen, G., Hannigan, J., Lambert, J.-C., Leblanc, T., McGee, T., Nedoluha, G., Petropavlovskikh, I., Seckmeyer, G., Simon, P., Steinbrecht, W., and Strahan, S.: The Network for the Detection of Atmospheric Composition Change (NDACC): History, status and perspectives, *Atmospheric Chemistry and Physics*, 18, 4935–4964, <https://doi.org/10.5194/acp-18-4935-2018>, 2018.

560 Dimitropoulou, E., Hendrick, F., Pinardi, G., Friedrich, M. M., Merlaud, A., Tack, F., De Longueville, H., Fayt, C., Hermans, C., Laffineur, Q., Fierens, F., and Van Roozendael, M.: Validation of TROPOMI tropospheric NO₂ columns using dual-scan MAX-DOAS measurements in Uccle, Brussels, *Atmospheric Measurement Techniques Discussions*, 2020, 1–50, <https://doi.org/10.5194/amt-2020-33>, <https://www.atmos-meas-tech-discuss.net/amt-2020-33/>, 2020.

565 Dirksen, R. J., Boersma, K. F., Eskes, H. J., Ionov, D. V., Bucsela, E. J., Levelt, P. F., and Kelder, H. M.: Evaluation of stratospheric NO₂ retrieved from the Ozone Monitoring Instrument: Intercomparison, diurnal cycle, and trending, *J. Geophys. Res.*, 116, D08 305, <https://doi.org/10.1029/2010jd014943>, 2011.

Drosoglou, T., Bais, A. F., Zyrichidou, I., Kouremeti, N., Poupkou, A., Liora, N., Giannaros, C., Eliassavet Koukouli, M., Balis, D., and Melas, D.: Comparisons of ground-based tropospheric NO₂ MAX-DOAS measurements to satellite observations with the aid of an air

570 quality model over the Thessaloniki area, Greece, *Atmospheric Chemistry and Physics*, 17, 5829–5849, <https://doi.org/10.5194/acp-17-5829-2017>, 2017.

Drosoglou, T., Koukouli, M. E., Kouremeti, N., Bais, A. F., and Zyrichidou, I.: MAX-DOAS NO₂ observations over Guangzhou, China; ground-based and satellite comparisons, *Atmos. Meas. Tech.*, 11, 2239–2255, 2018.

Errera, Q. and Fonteyn, D.: Four-dimensional variational chemical assimilation of CRISTA stratospheric measurements, *J. Geophys. Res.*, 575 106, 12,253–12,265, 2001.

ESA: Copernicus Sentinels 4 and 5 Mission Requirements Traceability Document, EOP-SM/2413/BV-bv, <https://sentinel.esa.int/documents/247904/2506504/Copernicus-Sentinels-4-and-5-Mission-Requirements-Traceability-Document.pdf>, 2017a.

ESA: Sentinel-5 Precursor Calibration and Validation Plan for the Operational Phase, ESA-EOPG-CSCOP-PL-0073, <https://sentinel.esa.int/documents/247904/2474724/Sentinel-5P-Calibration-and-Validation-Plan.pdf>, 2017b.

580 Eskes, H. J., van Geffen, J., Boersma, K. F., Sneep, M., ter Linden, M., Richter, A., Beirle, S., and Veefkind, J. P.: High spatial resolution nitrogen dioxide tropospheric column observations derived from Sentinel-5P TROPOMI observations, submitted to AMT, 2020.

Friedrich, M. M., Rivera, C., Stremme, W., Ojeda, Z., Arellano, J., Bezanilla, A., García-Reynoso, J. A., and Grutter, M.: NO₂ vertical profiles and column densities from MAX-DOAS measurements in Mexico City, *Atmospheric Measurement Techniques*, 12, 2545–2565, <https://doi.org/10.5194/amt-12-2545-2019>, <https://www.atmos-meas-tech.net/12/2545/2019/>, 2019.

585 Frieß, U., Beirle, S., Alvarado Bonilla, L., Bösch, T., Friedrich, M. M., Hendrick, F., Piters, A., Richter, A., van Roozendael, M., Rozanov, V. V., Spinei, E., Tirpitz, J.-L., Vlemmix, T., Wagner, T., and Wang, Y.: Intercomparison of MAX-DOAS vertical profile retrieval algorithms: studies using synthetic data, *Atmospheric Measurement Techniques*, 12, 2155–2181, <https://doi.org/10.5194/amt-12-2155-2019>, <https://www.atmos-meas-tech.net/12/2155/2019/>, 2019.

Gielen, C., Van Roozendael, M., Hendrick, F., Pinardi, G., Vlemmix, T., De Bock, V., De Backer, H., Fayt, C., Hermans, C., Gillotay, 590 D., and Wang, P.: A simple and versatile cloud-screening method for MAX-DOAS retrievals, *Atmospheric Measurement Techniques*, 7, 3509–3527, <https://doi.org/10.5194/amt-7-3509-2014>, <https://www.atmos-meas-tech.net/7/3509/2014/>, 2014.

Gratsea, M., Vrekoussis, M., Richter, A., Wittrock, F., Schönhardt, A., Burrows, J., Kazadzis, S., Mihalopoulos, N., and Gerasopoulos, E.: Slant column MAX-DOAS measurements of nitrogen dioxide, formaldehyde, glyoxal and oxygen dimer in the urban environment of Athens, *Atmospheric Environment*, 135, 118 – 131, <https://doi.org/https://doi.org/10.1016/j.atmosenv.2016.03.048>, <http://www.sciencedirect.com/science/article/pii/S1352231016302400>, 2016.

595 Griffin, D., Zhao, X., McLinden, C. A., Boersma, F., Bourassa, A., Dammers, E., Degenstein, D., Eskes, H., Fehr, L., Fioletov, V., Hayden, K., Kharol, S. K., Li, S.-M., Makar, P., Martin, R. V., Mihele, C., Mittermeier, R. L., Krotkov, N., Sneep, M., Lamsal, L. N., Linden, M. t., Geffen, J. v., Veefkind, P., and Wolde, M.: High-Resolution Mapping of Nitrogen Dioxide With TROPOMI: First Results and Validation Over the Canadian Oil Sands, *Geophys. Res. Lett.*, 46, 1049–1060, <https://doi.org/10.1029/2018GL081095>, 2019.

600 Gruzdev, A. N. and Elokhov, A. S.: Validation of Ozone Monitoring Instrument NO₂ measurements using ground based NO₂ measurements at Zvenigorod, Russia, *International Journal of Remote Sensing*, 31, 497–511, <https://doi.org/10.1080/01431160902893527>, <https://doi.org/10.1080/01431160902893527>, 2010.

Hendrick, F., Barret, B., Van Roozendael, M., Boesch, H., Butz, A., De Mazière, M., Goutail, F., Hermans, C., Lambert, J.-C., Pfeilsticker, K., and et al.: Retrieval of nitrogen dioxide stratospheric profiles from ground-based zenith-sky UV-visible observations: validation of the technique through correlative comparisons, *Atmos. Chem. Phys.*, 4, 2091–2106, <https://doi.org/10.5194/acp-4-2091-2004>, 2004.

Hendrick, F., Pommereau, J.-P., Goutail, F., Evans, R. D., Ionov, D., Pazmino, A., Kyrö, E., Held, G., Eriksen, P., Dorokhov, V., Gil, M., and Van Roozendael, M.: NDACC/SAOZ UV-visible total ozone measurements: improved retrieval and comparison with correlative ground-based and satellite observations, *Atmos. Chem. Phys.*, 11, 5975–5995, <https://doi.org/10.5194/acp-11-5975-2011>, 2011.

Hendrick, F., Müller, J.-F., Clémer, K., Wang, P., De Mazière, M., Fayt, C., Gielen, C., Hermans, C., Ma, J. Z., Pinardi, G., Stavrakou, T.,
610 Vlemmix, T., and Van Roozendael, M.: Four years of ground-based MAX-DOAS observations of HONO and NO₂ in the Beijing area, *Atmospheric Chemistry and Physics*, 14, 765–781, <https://doi.org/10.5194/acp-14-765-2014>, <http://www.atmos-chem-phys.net/14/765/2014/>, 2014.

Herman, J., Cede, A., Spinei, E., Mount, G., Tzortziou, M., and Abuhassan, N.: NO₂ column amounts from ground-based Pandora and MFDOAS spectrometers using the direct-sun DOAS technique: Intercomparisons and application to OMI validation, *Journal of Geophysical Research: Atmospheres*, 114, <https://doi.org/10.1029/2009JD011848>, <https://agupubs.onlinelibrary.wiley.com/doi/abs/10.1029/2009JD011848>, 2009.

Herman, J., Abuhassan, N., Kim, J., Kim, J., Dubey, M., Raponi, M., and Tzortziou, M.: Underestimation of column NO₂ amounts from the OMI satellite compared to diurnally varying ground-based retrievals from multiple PANDORA spectrometer instruments, *Atmos. Meas. Tech.*, 12, 5593–5612, <https://doi.org/10.5194/amt-12-5593-2019>, 2019.

Hönninger, G. and Platt, U.: Observations of BrO and its vertical distribution during surface ozone depletion at Alert, *Atmospheric Environment*, 36, 2481 – 2489, [https://doi.org/https://doi.org/10.1016/S1352-2310\(02\)00104-8](https://doi.org/10.1016/S1352-2310(02)00104-8), air/Snow/Ice Interactions in the Arctic: Results from ALERT 2000 and SUMMIT 2000, 2002.

Hönninger, G., von Friedeburg, C., and Platt, U.: Multi axis differential optical absorption spectroscopy (MAX-DOAS), *Atmospheric Chemistry and Physics*, 4, 231–254, www.atmos-chem-phys.org/acp/4/231/, 2004.

Hoque, H. M. S., Irie, H., Damiani, A., Rawat, P., and Naja, M.: First Simultaneous Observations of Formaldehyde and Glyoxal by MAX-DOAS in the Indo-Gangetic Plain Region, *SOLA*, 14, 159–164, <https://doi.org/10.2151/sola.2018-028>, 2018.

Ialongo, I., Virta, H., Eskes, H., Hovila, J., and Douros, J.: Comparison of TROPOMI/Sentinel-5 Precursor NO₂ observations with ground-based measurements in Helsinki, *Atmos. Meas. Tech.*, 13, 205–218, <https://doi.org/10.5194/amt-13-205-2020>, 2020.

Ionov, D. V., Timofeyev, Y. M., Sinyakov, V. P., Semenov, V. K., Goutail, F., Pommereau, J.-P., Bucsela, E. J., Celarier, E. A., and Kroon,
630 M.: Ground-based validation of EOS-Aura OMI NO₂ vertical column data in the midlatitude mountain ranges of Tien Shan (Kyrgyzstan) and Alps (France), *J. Geophys. Res.*, 113, D15S08, <https://doi.org/10.1029/2007jd008659>, 2008.

Irie, H., Kanaya, Y., Akimoto, H., Tanimoto, H., Wang, Z., Gleason, J. F., and Bucsela, E. J.: Validation of OMI tropospheric NO₂ column data using MAX-DOAS measurements deep inside the North China Plain in June 2006: Mount Tai Experiment 2006, *Atmospheric Chemistry and Physics*, 8, 6577–6586, <https://doi.org/10.5194/acp-8-6577-2008>, <http://www.atmos-chem-phys.net/8/6577/2008/>, 2008.

Irie, H., Takashima, H., Kanaya, Y., Boersma, K. F., Gast, L., Wittrock, F., Brunner, D., Zhou, Y., and Van Roozendael, M.: Eight-component retrievals from ground-based MAX-DOAS observations, *Atmospheric Measurement Techniques*, 4, 1027–1044, <https://doi.org/10.5194/amtd-4-639-2011>, <http://www.atmos-meas-tech-discuss.net/4/639/2011/>, 2011.

Irie, H., Boersma, K. F., Kanaya, Y., Takashima, H., Pan, X., and Wang, Z. F.: Quantitative bias estimates for tropospheric NO₂ columns retrieved from SCIAMACHY, OMI, and GOME-2 using a common standard for East Asia, *Atmospheric Measurement Techniques*, 5, 2403–2411, <https://doi.org/10.5194/amt-5-2403-2012>, <https://www.atmos-meas-tech.net/5/2403/2012/>, 2012.

Irie, H., Nakayama, T., Shimizu, A., Yamazaki, A., Nagai, T., Uchiyama, A., Zaizen, Y., Kagamitani, S., and Matsumi, Y.: Evaluation of MAX-DOAS aerosol retrievals by coincident observations using CRDS, lidar, and sky radiometer in Tsukuba, Japan, *Atmospheric Measurement Techniques*, 8, 2775–2788, <https://doi.org/10.5194/amt-8-2775-2015>, <https://www.atmos-meas-tech.net/8/2775/2015/>, 2015.

645 Jin, J., Ma, J., Lin, W., Zhao, H., Shaiganfar, R., Beirle, S., and Wagner, T.: MAX-DOAS measurements and satellite validation of tropospheric NO₂ and SO₂ vertical column densities at a rural site of North China, *Atmospheric Environment*, 133, 12 – 25, [https://doi.org/https://doi.org/10.1016/j.atmosenv.2016.03.031](https://doi.org/10.1016/j.atmosenv.2016.03.031), <http://www.sciencedirect.com/science/article/pii/S1352231016302011>, 2016.

Judd, L. M., Al-Saadi, J. A., Janz, S. J., Kowalewski, M. G., Pierce, R. B., Szykman, J. J., Valin, L. C., Swap, R., Cede, A., Mueller, M.,
650 Tiefengraber, M., Abuhassan, N., and Williams, D.: Evaluating the impact of spatial resolution on tropospheric NO₂ column comparisons within urban areas using high-resolution airborne data, *Atmos. Meas. Tech.*, 12, 6091–6111, <https://doi.org/10.5194/amt-12-6091-2019>, 2019.

Kanaya, Y., Irie, H., Takashima, H., Iwabuchi, H., Akimoto, H., Sudo, K., Gu, M., Chong, J., Kim, Y. J., Lee, H., Li, A., Si, F., Xu, J., Xie, P.-H., Liu, W.-Q., Dzhola, A., Postylyakov, O., Ivanov, V., Grechko, E., Terpugova, S., and Panchenko, M.: Long-term MAX-
655 DOAS network observations of NO₂ in Russia and Asia (MADRAS) during 2007–2012: instrumentation, elucidation of climatology, and comparisons with OMI satellite observations and global model simulations, *Atmospheric Chemistry and Physics*, 14, 7909–7927, <https://doi.org/10.5194/acp-14-7909-2014>, <http://www.atmos-chem-phys-discuss.net/14/2883/2014/>, 2014.

Kollonige, D. E., Thompson, A. M., Josipovic, M., Tzortziou, M., Beukes, J. P., Burger, R., Martins, D. K., van Zyl, P. G., Vakkari, V., and Laakso, L.: OMI Satellite and Ground-Based Pandora Observations and Their Application to Surface NO₂ Estimations at Terrestrial and
660 Marine Sites, *J. Geophys. Res. Atmos.*, 123, 1441–1459, <https://doi.org/10.1002/2017JD026518>, 2018.

Kreher, K., Van Roozendael, M., Hendrick, F., Apituley, A., Dimitropoulou, E., Frieß, U., Richter, A., Wagner, T., Abuhassan, N., Ang, L.,
Anguas, M., Bais, A., Benavent, N., Bösch, T., Bognar, K., Borovski, A., Bruchkouski, I., Cede, A., Chan, K. L., Donner, S., Drosoglou, T.,
Fayt, C., Finkenzeller, H., Garcia-Nieto, D., Gielen, C., Gómez-Martín, L., Hao, N., Herman, J. R., Hermans, C., Hoque, S., Irie, H., Jin, J.,
Johnston, P., Khayyam Butt, J., Khokhar, F., Koenig, T. K., Kuhn, J., Kumar, V., Lampel, J., Liu, C., Ma, J., Merlaud, A., Mishra, A. K.,
665 Müller, M., Navarro-Comas, M., Ostendorf, M., Pazmino, A., Peters, E., Pinardi, G., Pinharanda, M., Piters, A., Platt, U., Postylyakov, O.,
Prados-Roman, C., Puentedura, O., Querel, R., Saiz-Lopez, A., Schönhardt, A., Schreier, S. F., Seyler, A., Sinha, V., Spinei, E., Strong, K.,
Tack, F., Tian, X., Tiefengraber, M., Tirpitz, J.-L., van Gent, J., Volkamer, R., Vrekoussis, M., Wang, S., Wang, Z., Wenig, M., Wittrock, F.,
Xie, P. H., Xu, J., Yela, M., Zhang, C., and Zhao, X.: Intercomparison of NO₂, O₄, O₃ and HCHO slant column measurements by MAX-
DOAS and zenith-sky UV-Visible spectrometers during the CINDI-2 campaign, *Atmospheric Measurement Techniques Discussions*, 2019,
670 1–58, <https://doi.org/10.5194/amt-2019-157>, <https://www.atmos-meas-tech-discuss.net/amt-2019-157/>, 2019.

Lambert, J.-C., Van Roozendael, M., De Maziere, M., Simon, P., Pommereau, J.-P., Goutail, F., Sarkissian, A., Denis, L., Dorokhov, V.,
Eriksen, P., Kyrö, E., Leveau, J., Roscoe, H., Tellefsen, C., and Vaughan, G.: Pole to pole Validation of the ERS-2 GOME Level 2 Products
with the SAOZ Ground-based Network, *Proc. 3rd ESA ERS Scientific Symposium*, Florence, Italy, 17-20 March 1997, ESA SP-414, 2,
629–636, 1997a.

675 Lambert, J.-C., Van Roozendael, M., Granville, J., Gerard, P., Peeters, P., Simon, P., Claude, H., and Stahelin, J.: Comparison of the GOME
ozone and NO₂ total amounts at mid-latitude with ground-based zenith-sky measurements, *Atmospheric Ozone - 18th Quad. Ozone
Symp.*, L'Aquila, Italy, 1996, R. Bojkov and G. Visconti (Eds.), 1, 301–304, 1997b.

Lambert, J.-C., De Clercq, C., and von Clarmann, T.: Comparing and merging water vapour observations: A multi-dimensional perspective
on smoothing and sampling issues, in "Monitoring Atmospheric Water Vapour: Ground-Based Remote Sensing and In-situ Methods",

680 N. Kämpfer (Ed.), ISSI Scientific Report Series, Vol. 10, pp. 177–199, https://doi.org/10.1007/978-1-4614-3909-7_2, ISBN 978-1-4614-3908-0, © Springer New York, 2012.

685 Leitão, J., Richter, A., Vrekoussis, M., Kokhanovsky, A., Zhang, Q. J., Beekmann, M., and Burrows, J. P.: On the improvement of NO₂ satellite retrievals – aerosol impact on the airmass factors, *Atmospheric Measurement Techniques*, 3, 475–493, <https://doi.org/10.5194/amt-3-475-2010>, <https://amt.copernicus.org/articles/3/475/2010/>, 2010.

690 685 Levelt, P. F., Joiner, J., Tamminen, J., Veefkind, J. P., Bhartia, P. K., Stein Zweers, D. C., Duncan, B. N., Streets, D. G., Eskes, H., van der A, R., McLinden, C., Fioletov, V., Carn, S., de Laat, J., DeLand, M., Marchenko, S., McPeters, R., Ziemke, J., Fu, D., Liu, X., Pickering, K., Apituley, A., González Abad, G., Arola, A., Boersma, F., Chan Miller, C., Chance, K., de Graaf, M., Hakkarainen, J., Hassinen, S., Ialongo, I., Kleipool, Q., Krotkov, N., Li, C., Lamsal, L., Newman, P., Nowlan, C., Suleiman, R., Tilstra, L. G., Torres, O., Wang, H., and Wargan, K.: The Ozone Monitoring Instrument: overview of 14 years in space, *Atmospheric Chemistry and Physics*, 18, 5699–5745, <https://doi.org/10.5194/acp-18-5699-2018>, <https://www.atmos-chem-phys.net/18/5699/2018/>, 2018.

695 Lin, J.-T., Martin, R. V., Boersma, K. F., Sneep, M., Stammes, P., Spurr, R., Wang, P., Van Roozendael, M., Clément, K., and Irie, H.: Retrieving tropospheric nitrogen dioxide from the Ozone Monitoring Instrument: effects of aerosols, surface reflectance anisotropy, and vertical profile of nitrogen dioxide, *Atmospheric Chemistry and Physics*, 14, 1441–1461, <https://doi.org/10.5194/acp-14-1441-2014>, <https://www.atmos-chem-phys.net/14/1441/2014/>, 2014.

700 695 Liu, M., Lin, J., Boersma, K. F., Pinardi, G., Wang, Y., Chimot, J., Wagner, T., Xie, P., Eskes, H., Van Roozendael, M., Hendrick, F., Wang, P., Wang, T., Yan, Y., Chen, L., and Ni, R.: Improved aerosol correction for OMI tropospheric NO₂ retrieval over East Asia: constraint from CALIOP aerosol vertical profile, *Atmospheric Measurement Techniques*, 12, 1–21, <https://doi.org/10.5194/amt-12-1-2019>, <https://www.atmos-meas-tech.net/12/1/2019/>, 2019a.

705 Liu, M., Lin, J., Kong, H., Boersma, K. F., Eskes, H., Kanaya, Y., He, Q., Tian, X., Qin, K., Xie, P., Spurr, R., Ni, R., Yan, Y., Weng, H., and Wang, J.: A new TROPOMI product for tropospheric NO₂ columns over East Asia with explicit aerosol corrections, *Atmospheric Measurement Techniques Discussions*, 2020, 1–22, <https://doi.org/10.5194/amt-2019-500>, <https://www.atmos-meas-tech-discuss.net/amt-2019-500/>, 2020.

710 705 Liu, S., Valks, P., Pinardi, G., De Smedt, I., Yu, H., Beirle, S., and Richter, A.: An improved total and tropospheric NO₂ column retrieval for GOME-2, *Atmospheric Measurement Techniques*, 12, 1029–1057, <https://doi.org/10.5194/amt-12-1029-2019>, <https://www.atmos-meas-tech.net/12/1029/2019/>, 2019b.

Lorente, A., Boersma, K. F., Eskes, H. J., Veefkind, J. P., van Geffen, J. H. G. M., de Zeeuw, M. B., Denier van der Gon, H. A. C., Beirle, S., and Krol, M. C.: Quantification of nitrogen oxides emissions from build-up of pollution over Paris with TROPOMI, *Sci. Rep.*, 9, <https://doi.org/https://doi.org/10.1038/s41990-019-56428-5>, 2019.

715 Ma, J. Z., Beirle, S., Jin, J. L., Shaiganfar, R., Yan, P., and Wagner, T.: Tropospheric NO₂ vertical column densities over Beijing: results of the first three years of ground-based MAX-DOAS measurements (2008–2011) and satellite validation, *Atmospheric Chemistry and Physics*, 13, 1547–1567, <https://doi.org/10.5194/acp-13-1547-2013>, <https://www.atmos-chem-phys.net/13/1547/2013/>, 2013.

720 Nowlan, C. R., Liu, X., Janz, S. J., Kowalewski, M. G., Chance, K., Follette-Cook, M. B., Fried, A., González Abad, G., Herman, J. R., Judd, L. M., Kwon, H.-A., Loughner, C. P., Pickering, K. E., Richter, D., Spinei, E., Walega, J., Weibring, P., and Weinheimer, A. J.: Nitrogen dioxide and formaldehyde measurements from the GEOstationary Coastal and Air Pollution Events (GEO-CAPE) Airborne Simulator over Houston, Texas, *Atmos. Meas. Tech.*, 11, 5941–5964, <https://doi.org/10.5194/amt-11-5941-2018>, 2018.

Noxon, J. F., Whipple Jr., E. C., and Hyde, R. S.: Stratospheric NO₂: 1. Observational method and behavior at mid-latitude, *Journal of Geophysical Research*, 84, 5047–5065, <https://doi.org/10.1029/JC084iC08p05047>, 1979.

Ortega, I., Koenig, T., Sinreich, R., Thomson, D., and Volkamer, R.: The CU 2-D-MAX-DOAS instrument – Part 1: Retrieval of 3-D distributions of NO₂ and azimuth-dependent OVOC ratios, *Atmospheric Measurement Techniques*, 8, 2371–2395, <https://doi.org/10.5194/amt-8-2371-2015>, <https://www.atmos-meas-tech.net/8/2371/2015/>, 2015.

720 Peters, E., Ostendorf, M., Bösch, T., Seyler, A., Schönhardt, A., Schreier, S. F., Henzing, J. S., Wittrock, F., Richter, A., Vrekoussis, M., and Burrows, J. P.: Full-azimuthal imaging-DOAS observations of NO₂ and O₄ during CINDI-2, *Atmospheric Measurement Techniques*, 12, 4171–4190, <https://doi.org/10.5194/amt-12-4171-2019>, <https://www.atmos-meas-tech.net/12/4171/2019/>, 2019.

Petritoli, A., Giovanelli, G., Kostadinov, I., Ravegnani, F., Bortoli, D., Werner, R., Valev, D., and Atanassov, A.: SCIAMACHY validation 725 of NO₂ total column by means of ground-based DOAS measurements at Mt. Cimone (44N, 11E) and Stara Zagora (42N, 25E) stations, European Space Agency, Special Publication, NA, 2003.

Pfeilsticker, K., Arlander, D., Burrows, J., Erle, F., Gil, M., Goutail, F., Hermans, C., Lambert, J.-C., Platt, U., Pommereau, J.-P., Richter, 730 Sarkissian, A., Van Roozendael, M., Wagner, and Winterrath: Intercomparison of the influence of tropospheric clouds on UV-visible absorptions detected during the NDSC Intercomparison Campaign at OHP in June 1996, *Geophysical Research Letters*, 26, 1169–1172, <https://doi.org/10.1029/1999GL900198>, 1999.

Pinardi, G., Van Roozendael, M., Hendrick, F., Theys, N., Abuhassan, N., Bais, A., Boersma, F., Cede, A., Chong, J., Donner, S., Drosoglou, 735 T., Frieß, U., Granville, J., Herman, J. R., Eskes, H., Holla, R., Hovila, J., Irie, H., Kanaya, Y., Karagkiozidis, D., Kouremeti, N., Lambert, J.-C., Ma, J., Peters, E., Piters, A., Postylyakov, O., Richter, A., Remmers, J., Takashima, H., Tiefengraber, M., Valks, P., Vlemmix, T., Wagner, T., and Wittrock, F.: Validation of tropospheric NO₂ column measurements of GOME-2A and OMI using MAX-DOAS and direct sun network observations, *Atmospheric Measurement Techniques Discussions*, 2020, 1–55, <https://doi.org/10.5194/amt-2020-76>, <https://www.atmos-meas-tech-discuss.net/amt-2020-76/>, 2020.

Piters, A. J. M., Boersma, K. F., Kroon, M., Hains, J. C., Van Roozendael, M., Wittrock, F., Abuhassan, N., Adams, C., Akrami, M., Allaart, 740 M. A. F., Apituley, A., Beirle, S., Bergwerff, J. B., Berkhou, A. J. C., Brunner, D., Cede, A., Chong, J., Clémer, K., Fayt, C., Frieß, U., Gast, L. F. L., Gil-Ojeda, M., Goutail, F., Graves, R., Griesfeller, A., Großmann, K., Hemerijckx, G., Hendrick, F., Henzing, B., Herman, J., Hermans, C., Hoexum, M., van der Hoff, G. R., Irie, H., Johnston, P. V., Kanaya, Y., Kim, Y. J., Klein Baltink, H., Kreher, K., de Leeuw, G., Leigh, R., Merlaud, A., Moerman, M. M., Monks, P. S., Mount, G. H., Navarro-Comas, M., Oetjen, H., Pazmino, A., Perez-Camacho, M., Peters, E., du Piesanie, A., Pinardi, G., Puentedura, O., Richter, A., Roscoe, H. K., Schönhardt, A., Schwarzenbach, B., Shaiganfar, R., Sluis, W., Spinei, E., Stolk, A. P., Strong, K., Swart, D. P. J., Takashima, H., Vlemmix, T., Vrekoussis, M., Wagner, T., Whyte, C., Wilson, K. M., Yela, M., Yilmaz, S., Zieger, P., and Zhou, Y.: The Cabauw Intercomparison campaign for Nitrogen Dioxide measuring Instruments 745 (CINDI): design, execution, and early results, *Atmospheric Measurement Techniques*, 5, 457–485, <https://doi.org/10.5194/amt-5-457-2012>, <https://www.atmos-meas-tech.net/5/457/2012/>, 2012.

Platt, U. and Perner, D.: Measurements of atmospheric trace gases by long path differential UV-visible absorption spectroscopy, *Optical and Laser Remote Sensing*, edited by D.A. Killinger, and A. Mooradien, Springer Verlag, New York, pp. 95–105, 1983.

Pommereau, J. and Goutail, F.: O₃ and NO₂ ground-based measurements by visible spectrometry during Arctic winter and spring 1988, 750 *Geophys. Res. Lett.*, 15, 891–894, <https://doi.org/10.1029/GL015i008p00891>, 1988.

Robles-Gonzalez, C., Navarro-Comas, M., Puentedura, O., Schneider, M., Hase, F., Garcia, O., Blumenstock, T., and Gil-Ojeda, M.: Intercomparison of stratospheric nitrogen dioxide columns retrieved from ground-based DOAS and FTIR and satellite DOAS instruments over the subtropical Izana station, *Atmospheric Measurement Techniques*, 9, 4471–4485, <https://doi.org/10.5194/amt-9-4471-2016>, <https://www.atmos-meas-tech.net/9/4471/2016/>, 2016.

755 Roscoe, H., Johnston, P., Van Roozendael, M., Richter, A., Sarkissian, A., Roscoe, J., Preston, K., Lambert, J.-C., Hermans, C., De Cuyper, W., Dzienus, S., Winterrath, T., Burrows, J., Goutail, F., Pommereau, J.-P. D'Almeida, E., Hottier, J., Coureul, C., Ramon, D., Pundt, I., Bartlett, L., McElroy, C., Kerr, J., Elokhov, A., Giovanelli, G., Ravegnani, F., Premuda, M., Kostadinov, I., Erle, F., Wagner, T., Pfeilsticker, K., Kenntner, M., Marquard, L., Gil, M., Puentedura, O., Yela, M., Arlander, W., Kåstad Høiskar, B., Tellefsen, C., Karlsen Tørnkvist, K., Heese, B., Jones, R., Aliwell, S., and Freshwater, R.: Slant column measurements of O₃ and NO₂ during the NDSC intercomparison of zenith-sky UV-visible spectrometers in June 1996, *Journal of Atmospheric Chemistry*, 32, 281–314, 1999.

760 Schreier, S. F., Richter, A., Peters, E., Ostendorf, M., Schmalwieser, A. W., Weihs, P., and Burrows, J. P.: Dual ground-based MAX-DOAS observations in Vienna, Austria: Evaluation of horizontal and temporal NO₂, HCHO, and CHOCHO distributions and comparison with independent data sets, *Atmospheric Environment: X*, 5, 100 059, <https://doi.org/https://doi.org/10.1016/j.aeaoa.2019.100059>, <http://www.sciencedirect.com/science/article/pii/S2590162119300620>, 2020.

765 Sinreich, R., Friess, U., Wagner, T., and Platt, U.: Multi axis differential optical absorption spectroscopy (MAX-DOAS) of gas and aerosol distributions., *Faraday discussions*, 130, 153–64; discussion 241–64, 519–24, 2005.

Solomon, S., Schmeltekopf, A. L., and Sanders, R. W.: On the interpretation of zenith sky absorption measurements, *J. Geophys. Res.*, 92, 8311–8319, <https://doi.org/10.1029/JD092iD07p08311>, 1987.

770 Tirpitz, J.-L., Frieß, U., Hendrick, F., Alberti, C., Allaart, M., Apituley, A., Bais, A., Beirle, S., Berkhou, S., Bognar, K., Bösch, T., Bruchkowski, I., Cede, A., Chan, K. L., den Hoed, M., Donner, S., Drosoglou, T., Fayt, C., Friedrich, M. M., Frumau, A., Gast, L., Gielen, C., Gomez-Martín, L., Hao, N., Hensen, A., Henzing, B., Hermans, C., Jin, J., Kreher, K., Kuhn, J., Lampel, J., Li, A., Liu, C., Liu, H., Ma, J., Merlaud, A., Peters, E., Pinardi, G., Piters, A., Platt, U., Puentedura, O., Richter, A., Schmitt, S., Spinei, E., Stein Zweers, D., Strong, K., Swart, D., Tack, F., Tiefengraber, M., van der Hoff, R., van Roozendael, M., Vlemmix, T., Vonk, J., Wagner, T., Wang, Y., Wang, Z., Wenig, M., Wiegner, M., Wittrock, F., Xie, P., Xing, C., Xu, J., Yela, M., Zhang, C., and Zhao, X.: Intercomparison of MAX-DOAS vertical profile retrieval algorithms: studies on field data from the CINDI-2 campaign, *Atmospheric Measurement Techniques Discussions*, 2020, 1–49, <https://doi.org/10.5194/amt-2019-456>, <https://www.atmos-meas-tech-discuss.net/amt-2019-456/>, 2020.

775 Tzortziou, M., Herman, J. R., Ahmad, Z., Loughner, C. P., Abuhassan, N., and Cede, A.: Atmospheric NO₂ dynamics and impact on ocean color retrievals in urban nearshore regions, *Journal of Geophysical Research: Oceans*, 119, 3834–3854, <https://doi.org/10.1002/2014JC009803>, 2014.

780 Valks, P., Pinardi, G., Richter, A., Lambert, J.-C., Hao, N., Loyola, D., Van Roozendael, M., and Emmadi, S.: Operational total and tropospheric NO₂ column retrieval for GOME-2, *Atmospheric Measurement Techniques*, 4, 1491–1514, <https://doi.org/10.5194/amt-4-1491-2011>, <https://www.atmos-meas-tech.net/4/1491/2011/>, 2011.

785 van Geffen, J., Boersma, K. F., Eskes, H., Sneep, M., ter Linden, M., Zara, M., and Veefkind, J. P.: S5P TROPOMI NO₂ slant column retrieval: method, stability, uncertainties and comparisons with OMI, *Atmospheric Measurement Techniques*, 13, 1315–1335, <https://doi.org/10.5194/amt-13-1315-2020>, <https://www.atmos-meas-tech.net/13/1315/2020/>, 2020.

Vandaele, A. C., Fayt, C., Hendrick, F., Hermans, C., Humbled, F., Van Roozendael, M., Gil, M., Navarro, M., Puentedura, O., Yela, M., Braathen, G., Stebel, K., Tørnkvist, K., Johnston, P., Kreher, K., Goutail, F., Mieville, A., Pommereau, J.-P., Khaikine, S., Richter, A., Oetjen, H., Wittrock, F., Bugarski, S., Frieß, U., Pfeilsticker, K., Sinreich, R., Wagner, T., Corlett, G., and Leigh, R.: An intercomparison campaign of ground-based UV-visible measurements of NO₂, BrO, and OCIO slant columns: Methods of analysis and results for NO₂, *J. Geophys. Res. Atmos.*, 110, <https://doi.org/10.1029/2004JD005423>, 2005.

790

Verhoelst, T., Granville, J., Hendrick, F., Köhler, U., Lerot, C., Pommereau, J.-P., Redondas, A., Van Roozendael, M., and Lambert, J.-C.: Metrology of ground-based satellite validation: co-location mismatch and smoothing issues of total ozone comparisons, *Atmos. Meas. Tech.*, 8, 5039–5062, <https://doi.org/10.5194/amt-8-5039-2015>, 2015.

Vlemmix, T., Piters, A. J. M., Stammes, P., Wang, P., and Levelt, P. F.: Retrieval of tropospheric NO₂ using the MAX-DOAS method combined with relative intensity measurements for aerosol correction, *Atmospheric Measurement Techniques*, 3, 1287–1305, <https://doi.org/10.5194/amt-3-1287-2010>, <https://www.atmos-meas-tech.net/3/1287/2010/>, 2010.

Vlemmix, T., Eskes, H. J., Piters, A. J. M., Schaap, M., Sauter, F. J., Kelder, H., and Levelt, P. F.: MAX-DOAS tropospheric nitrogen dioxide column measurements compared with the Lotos-Euros air quality model, *Atmospheric Chemistry and Physics*, 15, 1313–1330, <https://doi.org/10.5194/acp-15-1313-2015>, <https://www.atmos-chem-phys.net/15/1313/2015/>, 2015.

795 Wagner, T., Beirle, S., Brauers, T., Deutschmann, T., Frieß, U., Hak, C., Halla, J. D., Heue, K. P., Junkermann, W., Li, X., Platt, U., and Pundt-Gruber, I.: Inversion of tropospheric profiles of aerosol extinction and HCHO and NO₂ mixing ratios from MAX-DOAS observations in Milano during the summer of 2003 and comparison with independent data sets, *Atmos. Meas. Tech.*, 4, 2685–2715, 2011.

800 Wang, Y., Li, A., Xie, P. H., Wagner, T., Chen, H., Liu, W. Q., and Liu, J. G.: A rapid method to derive horizontal distributions of trace gases and aerosols near the surface using multi-axis differential optical absorption spectroscopy, *Atmospheric Measurement Techniques*, 7, 1663–1680, <https://doi.org/10.5194/amt-7-1663-2014>, <https://www.atmos-meas-tech.net/7/1663/2014/>, 2014.

805 Wang, Y., Beirle, S., Lampel, J., Koukouli, M., De Smedt, I., Theys, N., Li, A., Wu, D., Xie, P., Liu, C., Van Roozendael, M., Stavrakou, T., Müller, J.-F., and Wagner, T.: Validation of OMI, GOME-2A and GOME-2B tropospheric NO₂, SO₂ and HCHO products using MAX-DOAS observations from 2011 to 2014 in Wuxi, China: investigation of the effects of priori profiles and aerosols on the satellite products, *Atmospheric Chemistry and Physics*, 17, 5007–5033, <https://doi.org/10.5194/acp-17-5007-2017>, <https://www.atmos-chem-phys.net/17/5007/2017/>, 2017.

810 Xing, C., Liu, C., Wang, S., Chan, K. L., Gao, Y., Huang, X., Su, W., Zhang, C., Dong, Y., Fan, G., Zhang, T., Chen, Z., Hu, Q., Su, H., Xie, Z., and Liu, J.: Observations of the vertical distributions of summertime atmospheric pollutants and the corresponding ozone production in Shanghai, China, *Atmospheric Chemistry and Physics*, 17, 14 275–14 289, <https://doi.org/10.5194/acp-17-14275-2017>, <https://www.atmos-chem-phys.net/17/14275/2017/>, 2017.

815 Xing, C., Liu, C., Hu, Q., Fu, Q., Lin, H., Wang, S., Su, W., Wang, W., Javed, Z., and Liu, J.: Identifying the wintertime sources of volatile organic compounds (VOCs) from MAX-DOAS measured formaldehyde and glyoxal in Chongqing, southwest China, *Science of The Total Environment*, 715, 136 258, <https://doi.org/https://doi.org/10.1016/j.scitotenv.2019.136258>, <http://www.sciencedirect.com/science/article/pii/S0048969719362540>, 2020.

820 Yela, M., Gil-Ojeda, M., Navarro-Comas, M., Gonzalez-Bartolomé, D., Puentedura, O., Funke, B., Iglesias, J., Rodríguez, S., García, O., Ochoa, H., and Deferrari, G.: Hemispheric asymmetry in stratospheric NO₂ trends, *Atmospheric Chemistry and Physics*, 17, 13 373–13 389, <https://doi.org/10.5194/acp-17-13373-2017>, <https://www.atmos-chem-phys.net/17/13373/2017/>, 2017.

825 Zhao, X., Griffin, D., Fioletov, V., McLinden, C., Cede, A., Tiefengraber, M., Müller, M., Bognar, K., Strong, K., Boersma, F., Eskes, H., Davies, J., Ogyu, A., and Lee, S. C.: Assessment of the quality of TROPOMI high-spatial-resolution NO₂ data products, *Atmospheric Measurement Techniques Discussions*, 2019, 1–48, <https://doi.org/10.5194/amt-2019-416>, <https://www.atmos-meas-tech-discuss.net/amt-2019-416/>, 2019.